A Four-Compartment Multiscale Model of Fluid and Drug Distribution in Vascular Tumours

R.J. Shipley[1⋆], P.W. Sweeney[1], S.J. Chapman[2], T. Roose[3]

1: Department of Mechanical Engineering, University College London, Torrington Place, London, WC1E 7JE.

2: Oxford Centre for Industrial and Applied Mathematics, Mathematical Institute, 24–29 St. Giles', Oxford OX1 3LB.

3: School of Engineering Sciences, Faculty of Engineering and Physical Sciences, University of Southampton, Highfield, Southampton SO17 1BJ.

⋆: Corresponding author

Abstract

It is vital to elucidate the subtle relationship between vascular network structure and mass transport to predict and improve the efficacy of anti-cancer treatments. In this paper, mathematical homogenization is used to derive a new multiscale continuum model of blood and chemotherapy transport in the arteriole, capillary and venule networks, and interstitium of a vascular tumour. This model and framework enables information at a range of vascular hierarchies to be fed into an effective description on the length scale of the tumour. The model is explored in a case study of a simple geometry representative of a tumour in a dorsal skinfold geometry setup. Specifically, we explore the role of vascular network architecture in influencing fluid and drug perfusion on the length scale of the chamber. A single parameter, P, is identified that relates tumour-scale fluid perfusion to the permeability and density of the capillary bed. By fixing the topological and physiological properties of the arteriole and venule networks, an optimal value for P is identified which maximises tumor fluid transport and is thus hypothesized to benefit chemotherapy delivery. We calculate the values for P for eight explicit network structures; in each case vascular intervention by either decreasing the permeability, or increasing the density, of the capillary network would increase fluid perfusion through the cancerous tissue. Chemotherapy delivery via either a single injection or constant perfusion in a idealised, two-dimensional tumour, representative of an *in vivo* testing setup, is compared; single injection is consistently more successful compared to constant perfusion, and the model outputs predict when to deliver a second dose. These results highlight the potential of computational modelling to elucidate the link between vascular architecture and fluid, drug distribution in tumours.

Key Words

mathematical modelling homogenization vasculature cancer chemotherapy

1 Introduction

Solid tumours are characterized by an abnormal microenvironment that distinguishes them from healthy tissue and reduces drug delivery to the cancerous tissue. This is a consequence of numerous factors that include a poorly organized vascular architecture, irregular blood flow and the compression of blood and lymphatic vessels by cancer cells [11]. The spatial and temporal heterogeneities in blood supply coupled with variations in the vascular morphology at both microscopic and macroscopic levels cause the spatial distribution of therapeutic agents in tumours to be heterogeneous. Drug treatments (mainly antiangiogenics such as avastin, but also vascular disrupting and regularising agents such as combretastatins and nelfinavir, respectively) have been developed specifically to target the abnormal vasculature in tumours; however, their impact is hard to predict as the relationship between network structure and the functional parameters that determine mass transport is subtle. For example, increasing the number or diameter of vessels can impair the blood flow distribution, whilst inhibiting angiogenesis is hypothesized to improve circulation [20]; in addition, tumours have been shown to display resistance to vascular disruption therapy via physical mechanisms, such network connectivity and redundancy [7].

The quality and volume of data characterizing tissue vascular architecture is increasing, and it is now possible to describe vascular structure in a highly detailed way. As the resolution of this data continues to increase, it may become too computationally intensive to simulate flow and mass transport in the entire vascular tree using a discrete approach where vessels are treated individually. In addition, in order to interpret the results they must not be too sensitive to the full vascular geometry, but only to some key characteristics of it. One approach is to employ continuum models in which imaging data are used to deduce functional properties relevant to blood and mass transport. The mathematical process of homogenization [19] is one candidate for developing these continuum models, as it enables spatial heterogeneities at different scales to be transformed into a tractable tissue-scale model. Macro-(or tissue-)scale equations are derived by using a mathematical averaging process to incorporate the relevant micro-scale topological and model properties. The final macro-scale equations can be solved numerically, and are far less computationally expensive than solving the microscale equations throughout the domain. A well known example of mathematical homogenization in practice is Darcy's law; although it was first proposed as an empirical law by Darcy in 1856 (based on water flow experiments through beds of sand) [6], it was subsequently derived from the Stokes equations using homogenization techniques [9]. This homogenization approach enabled the influence of exact particle shape on hydraulic permeability to be determined.

The hierarchy of healthy vasculature consists of branching arterioles and venules, interconnected by a mesh-like network of capillaries embedded in the interstitium (comprised of cells, and extra-cellular and extra-vascular space). However, the hierarchical structure of arterioles and venules evident in healthy tissue is disrupted in tumors where it is well-established that tumour blood vessels are heterogeneous with regard to topology, function and structure [16]. Instead a complex tortuous network of angiogenic blood vessels exists which are fed and drained by large, often tortuous

blood vessels [17] which results in elevated interstitial fluid pressure [25] and poor drug penetration to the core of a tumor [10, 11, 7]. Here we use mathematical methods to explore this abnormal tumor microenvironment.

The method of homogenization is applicable to vascular networks with periodic micro-structure, and with disparate length scales apparent across tissue. This enables us to make progress towards a computationally tractable model whilst retaining key architectural information. Darcy's law has also been shown to provide good predictivity of macroscale fluid mechanics for non-periodic structures, even if the multiscale derivation assumes periodicity [4, 5]. Figure 1 shows representations of both the capillary or micro-scale, and the tissue- or macro-scale. On the micro-scale, both the capillaries and interstitium are identifiable, and are illustrated by periodic changes of dark and light purple regions, respectively. An example periodic unit cell is circled in red, which repeats in all directions (although the structure must be periodic in this sense, there is no other assumption of homogeneity within this unit). The capillary length scale is given by the typical inter-capillary distance, d. If the ratio between the capillary length scale, d, and the tumour or macro-scale, L is small, *i.e.* $\epsilon = d/L \ll 1$, it is possible to derive an effective macroscopic model describing both the capillaries and the interstitium. In the schematic on the left-hand side of Figure 1 the heterogeneities can be distinguished. By comparison, viewed from a distance, or from the tumour or macro-scale, the heterogeneities average out as shown in the right-hand side of Figure 1. Here, both the capillary network and interstitium can be represented as continua; therefore, the distribution of fluid in the two can be represented as a 'grey-scale'. This averaging to a continuum is exactly what the mathematical process of homogenization achieves. The space variable $\mathbf{x} = (x, y, z)$ reveals the properties of the system on the length scale of the tumour. Scaling $\mathbf{x}$ with ϵ^{-1} defines a new space variable $\mathbf{X} = (X, Y, Z) = \epsilon^{-1}\mathbf{x}$ which reflects the system properties at the capillary scale. One of the fundamental assumptions of homogenization is that ϵ is sufficiently small that the length variables $\mathbf{x}$ and $\mathbf{X}$ are disparate and can be treated as two independent variables [19].

In this paper we use multiscale mathematical models to investigate the dependence of fluid perfusion and drug distribution properties on vascular structure under two key assumptions. First of all we discretise the vascular tree according to vessel dimension, although in reality the topological properties of healthy vessels are continuously distributed from the arteries to the capillary bed, and to the veins. We divide the vascular tree into a supplying artery and draining vein, together with arteriole, venule and capillary networks, and categorise these networks by three different length scales. These are the length scale of the tissue, the arterioles and venules (a typical inter-arteriole or inter-venule separation), and the capillaries (a typical inter-capillary separation). In this way, the dependence of tumour-scale fluid and drug perfusion properties on vasculature structure can be seen as occurring through the interaction of the various length scales under consideration.

Second, we assume that the structure is spatially periodic on the capillary, arteriole and venule length scales. For example, on the length scale of the capillaries the tumour is comprised of a periodic array of capillaries embedded in the interstitium, as depicted in Figure 1. Although this is a simplifying assumption, the hierarchical vascular structure evident in healthy tissue rarely occurs in vascular tumors [16, 17]. Therefore, we assume an unstratified, periodic tumor

vasculature enabling continuum mathematical models to be derived using homogenization. These continuum models are computationally tractable compared to simulations throughout the vascular tree, and enable the impact of varying vascular structure on tumour-scale fluid perfusion and mass transport to be tested, without re-deriving the models each time. In the long-term, this will help to both elucidate the mechanisms underlying transport, and to quantify the impact of vascular structure on tumour-scale fluid and drug perfusion.

In [2, 23], we used homogenization to derive effective fluid and drug perfusion models for a capillary bed and surrounding interstitium. The final fluid equations comprised a double porous medium, with coupled Darcy flow through the interstitium and vasculature, whereas the drug equations comprised advection-reaction equations; in each case the dependence of the transport coefficients on the vascular geometry was determined by solving capillary-scale cell problems. In this paper we extend that approach to a four-component tissue structure, so that vascular hierarchy may be accounted for in the models. We derive a new set of effective equations for fluid and drug distribution, and explore the role of vascular architecture in determining tissue-scale fluid and drug perfusion using an example case study of a rodent model for monitoring of microvascular pathophysiology *in vivo* (a dorsal skinfold chamber.

2 The Model Setup

A dorsal skinfold chamber is the chronic implantation of an observation chamber on the dorsal skinfold of rodents which enables repeated, intravital microscopic observations [14]. These chambers are a common tool for therapy development, particularly for cancers. In this paper, we use a simplified representation of this chamber structure as a case study to explore implementation of the four-component transport model, and to explore the role of vascular architecture in determining effective parameters relating to fluid and drug delivery. Blood flow through a chamber containing cancerous tissue is captured by considering four separate components: the arteriole, venule and capillary networks, and the interstitium (comprised of cells, and extra-cellular and extra-vascular space). We assume that fluid flows from a seeded feeding artery, through the arterioles into the capillaries, then into the venules before leaving the chamber via a seeded draining vein. Since the capillaries are leaky there may also be fluid exchange between the capillaries and the interstitium. In our model, it is not possible for fluid to travel directly from the arterioles into the venules bypassing the capillaries. The fluid pathway is summarized in Figure 2. Throughout this paper, we assume that dorsal skinfold chambers do not have functioning lymphatics due to clamping of the chamber to the skin and general lack of lymphatics in tumors, and therefore neglect this aspect in the fluid transport models. Further, whilst difficulties exist in categorising blood vessels into distinct groups [17], for convenience, we divide the tumour vasculature into three separate components: arteriole, capillary and venule networks.

The model structure explained above can be described using three different length scales. The finest scale is referred to as the "micro-scale" or the "capillary length scale" and describes the capillaries and interstitium, characterized by a typical inter-capillary separation $d \approx 50\mu$m. The most course scale is referred to as the "chamber-scale" and describes

the scale of the entire chamber *i.e.* $L \approx 10^4 \mu\text{m} = 1\text{cm}$. In between these scales, we introduce a third length-scale which relates to the separate arteriole or venule networks, characterized by a typical vessel separation $s \approx 10^3 \mu\text{m}$. These three length scales are depicted in Figure 4, and interact through two dimensionless ratios

$$\nu = \frac{d}{s} \approx 5 \times 10^{-2}, \quad \eta = \frac{s}{L} \approx 10^{-1}. \tag{1}$$

On the chamber-scale, none of the arterioles, venules, capillaries or interstitium are distinguishable; however, a seeded artery and vein supply a pressure gradient across the vasculature. Zooming into any point on the chamber-scale reveals the arteriole and venule-scales. Here blood flows through the arterioles or venules and seeps into a porous tissue matrix comprised of capillaries and interstitium. Finally, zooming into a point in the tissue on the length scale of the arterioles and venules reveals the capillary-scale. Here blood flows through the capillary network and seeps into the interstitium.

As $\nu \ll 1$ the micro and arteriole/venule length scales are well-separated. Therefore, it is possible to use asymptotic homogenization to move from the micro- to the arteriole/venule descriptions and derive the porous medium equations for the capillary network and interstitium on the length scale of the arterioles and venules. Similarly $\eta \ll 1$, so we can move from the arteriole/venule to the chamber descriptions and derive the coupled porous medium equations that describe fluid transport in the arterioles, venules, capillaries and interstitium on the scale of the chamber.

Next we consider fluid and drug transport in turn. We present and analyse the fluid and drug transport problems on the length scale of the chamber, as well as a summary of the derivation steps using homogenization, including parameter estimation on each of the length scales described above.

2.1 Fluid Transport Model

We denote the fluid pressure by p and the velocity by $\mathbf{u}$, with subscripts a, v, c or t denoting the values of p or $\mathbf{u}$ in the arterioles, venules, capillaries and interstitium, respectively.

2.1.1 Fluid Transport on the Scale of the Capillaries

The capillaries of a tumour are embedded in the interstitium, which is itself comprised of cells and extra-cellular space. We assume the tumour occupies a 3-dimensional volume and can be described as spatially periodic on the capillary-scale. This structure is depicted by a 2D schematic in Figure 1, where a single periodic unit cell is highlighted in red. We denote the total volume of a unit cell by V, the volume of the capillaries in a unit by V_c, and the volume of the interstitium by V_t. We denote the fluid velocity by $\mathbf{u}$ and the pressure by p, with subscripts t or c denoting the interstitium or capillaries respectively. We assume that the flow in both the interstitium and the capillaries is incompressible. The interstitium is comprised of cells surrounded by extra-cellular space. However, the capillaries are much larger than the inter-cell separation of the interstitium, and so we treat the interstitium as an isotropic porous

medium and describe fluid flow through it by Darcy's law (*e.g.* [27, 28]). Therefore, in the interstitium

$$\boldsymbol{\nabla} \cdot \mathbf{u}_t = 0, \quad \mathbf{u}_t = -\frac{k^{int}}{\mu} \nabla p_t, \tag{2}$$

where k^{int} is the interstitial permeability and μ is the viscosity of blood plasma.

Blood flow in the capillaries of the microcirculation is a highly complex process. Healthy human blood is a concentrated suspension containing red blood cells (RBCs) at a concentration (haematocrit) of 40–45 %. In vessels much larger than the RBCs (*i.e.* with diameter much larger than $\approx 8\mu$m), blood can be treated as a continuum with a viscosity that is approximately constant. In vessels smaller than this, the finite size of RBCs results in non-continuum behaviour and complex rheology that causes several important effects *e.g.* the Fåhraeus [29] and Fåhraeus-Lindqvist [30, 38] effects, and phase separation at diverging bifurcations [37, 39]. Empirical laws have been developed to describe these non-Newtonian effects [38, 39] ,and these have also been incorporated into homogenization frameworks (for example, [44]). The introduction of more realistic haemodynamic descriptions of blood are important to predict tissue-scale fluid mechanics, and would result in an effective and spatially-dependent tissue-scale viscosity.

Due to the additional computational expense of incorporating non-Newtonian haemodynamics, and the emphasis here on the development and application of a new modelling framework, we neglect non-Newtonian effects here and assume that the fluid flow in the capillaries is described by the Navier-Stokes' equations for a fluid of constant viscosity. Therefore, in the capillaries we have

$$\boldsymbol{\nabla} \cdot \mathbf{u}_c = 0, \quad \rho \left(\frac{\partial \mathbf{u}_c}{\partial t} + (\mathbf{u}_c \cdot \boldsymbol{\nabla}) \, \mathbf{u}_c \right) = -\boldsymbol{\nabla} p_c + \mu \nabla^2 \mathbf{u}_c \tag{3}$$

where ρ is the fluid density. The leakage from the capillaries into the interstitium is given by Starling's law, $\mathbf{q}_e = L_p \, (p_c - p_t) \, \mathbf{n}$, where $\mathbf{q}_e$ is the leakage flux, L_p is the vascular permeability (assumed constant), $\mathbf{n}$ is the unit outward pointing normal to the capillary surface, and p_c, p_t are evaluated on the interior and exterior sides of the capillary wall respectively. Given this, we impose continuity of mass flux across the capillary walls, so that

$$\mathbf{u}_t \cdot \mathbf{n} = \mathbf{u}_c \cdot \mathbf{n} = L_p \, (p_c - p_t) \quad \text{on the capillary walls.} \tag{4}$$

Finally, we impose a no-slip condition on the capillary walls so that

$$\mathbf{u}_c \cdot \boldsymbol{\tau} = 0 \quad \text{on the capillary walls,} \tag{5}$$

where $\boldsymbol{\tau}$ is a unit tangential vector to the capillary wall. In practice there is slip at the capillary surface, and it is determined by the microvascular rheology, in particular the structure of the endothelial glycocalyx. Given that we have neglected non-Newtonian effects here, it is sensible to simplify to the no-slip boundary condition (5).

2.1.2 Parameter Estimation

Geometrical Parameters Geometrical data on capillaries are presented in [34, 35], with data on the capillaries, arterioles and venules in a dorsal skinfold chamber summarized in Table 1. A typical intercapillary distance d is $50\,\mu$m, whilst a representative mean inter-arteriole or inter-venule distance s is $10^3\mu$m. This gives a typical value of ν as 5×10^{-2}, justifying the assumption $\nu \ll 1$.

Physiological Parameters Experimental values of the hydraulic conductivity k^{int}/μ are determined in [31, 32, 43] for rat squamous cell tissue, hepatoma in vitro, mouse mammary carcinoma and rat hepatocarcinoma tissue; values lie in the range 10^{-9} to 10^{-6} cm^3 s kg^{-1}. However, these values are obtained by applying Darcy's law to *in vitro* filtration data; measuring the hydraulic conductivity *in vivo* is very difficult. The blood viscosity, μ, depends on the hematocrit (the density of red blood cells) and the temperature, and (though we are approximating blood as a Newtonian fluid) also on the shear rate. Nevertheless, for a normal 40% hematocrit and 37°C, $\mu \approx 4 \times 10^{-3}$ kg m^{-1}s^{-1} [40]. On this basis, the interstitial permeability k^{int} lies between 4×10^{-14} and 4×10^{-11} cm^2, although the range in practice is likely to be much larger, and highly dependent on the tissue type.

The vascular hydraulic permeability L_p can be difficult to estimate. In [42], the authors attempt to address this by measuring the capillary filtration coefficient. Using this technique, values for L_p can be extracted from the data in [32, 41] for mouse mammary carcinoma and healthy rat hindquarter tissue, and are about 10^{-6} cm^2 s kg^{-1}. Finally, the blood density $\rho \approx 1040$ kg m^{-3} [33] and we assume a typical velocity in the capillaries is $U \approx 25\ \mu$m s^{-1}.

There are three dimensionless parameters that characterize the fluid transport problem. First of all, the Reynolds number, $\mathrm{Re} = \rho U d/\mu$ represents the ratio of inertial to viscous forces in the capillaries. Therefore if inertia dominates over viscosity, Re is large, whereas if viscosity dominates over inertia, Re is small. Here we find that $\mathrm{Re} \approx 3.3 \times 10^{-4}$, and therefore the importance of inertia is negligible on the micro-scale. The final two dimensionless parameters are

$$\kappa = \frac{k^{int} s}{d^3} \quad \text{and} \quad R = \frac{\mu L_p s^3}{d^4}, \tag{6}$$

which represent the relative permeability of the interstitium and capillary walls, respectively, in comparison to fluid transport. We find that $R \approx 6.4 \times 10^{-5}$ and κ lies in the range 3.2×10^{-8} to 3.2×10^{-5}. The relative sizes of these parameters are important for the homogenization analysis. Specifically, the average fluid velocity on the length scale of the arterioles and venules will be dominated by that in the capillaries, and the contribution of the interstitium to the average fluid velocity is of size ν.

2.1.3 Fluid Transport on the Scale of the Arterioles and Venules

We homogenize the model for fluid transport in the capillaries and interstitium, given by equations (2)–(5), to give a description for transport in the capillaries and interstitium on the scale of the arterioles and venules. The homogenization steps are detailed in [23, 22] and may be summarised as (a) assuming length scale separation between the micro-

and arteriole/venule- length scales by substituting $\nabla = \nabla_{\text{micro}} + \nu\nabla_{\text{arteriole/venule}}$ in equations (2)–(5), (b) expanding all variables asymptotically in powers of ν, (c) equating coefficients of powers of ν in (2)–(5), (d) decomposing the fluid velocity $\mathbf{u}$ into components that vary on the micro- and arteriole/venule-scales, with the component relating to the micro problem being defined through a cell problem on the micro-scale geometry, (e) averaging over the micro-scale to derive the arteriole/venule-scale relationships. On the arteriole/venule length scale, the capillaries and interstitium appear as continua, and behave as a double porous medium with coupled Darcy flow between the two. The equations for fluid transport in the capillaries and interstitium, on this length scale, are

$$\mathbf{u}_c = -\frac{\eta}{\mu}\mathbf{K}\cdot\boldsymbol{\nabla}p_c\,, \quad \boldsymbol{\nabla}\cdot(\mathbf{K}\cdot\boldsymbol{\nabla}p_c) = 0, \quad \mathbf{u}_t = -\frac{\nu\eta}{\mu}\mathbf{E}\cdot\boldsymbol{\nabla}p_t\,, \quad \boldsymbol{\nabla}\cdot(\mathbf{E}\cdot\boldsymbol{\nabla}p_t) = \frac{RSd}{V_t}\left(p_t - p_c\right)\,, \tag{7}$$

where R (which is dimensionless) represents the leakiness of the capillary walls (and is given in (6)), and S/V_t is the ratio of the surface area of the capillaries to the volume of interstitium. Further, $\mathbf{K}$ and $\mathbf{E}$ are the fluid permeability tensors associated with the capillary network and interstitium, and are determined by the homogenization process. They are given explicitly at the end of this section in terms of two cell problems that must be solved on the length scale of the capillaries, once the capillary-scale geometry has been specified. It is precisely these permeability tensors $\mathbf{K}$ and $\mathbf{E}$ that relate transport on courser length scales to the geometry and transport properties on the capillary-scale.

On the length scale of the arterioles and venules, fluid flows from the arterioles into the porous tissue matrix (comprised of the capillary network and interstitium), and then into the venules; a schematic of this setup is shown in Figure 3. We denote the volume of arterioles and venules in a unit by V_a and V_v respectively, and the volume of porous tissue matrix by V_p. Equations (7) describe the fluid transport in the porous tissue matrix. We use subscripts a and v to denote the arterioles and venules, respectively, and describe blood flow in the arterioles and venules using the Navier-Stokes equations so that

$$\boldsymbol{\nabla}\cdot\mathbf{u}_i = 0, \quad \rho\left(\frac{\partial\mathbf{u}_i}{\partial t} + \left(\mathbf{u}_c\cdot\boldsymbol{\nabla}\right)\mathbf{u}_i\right) = -\boldsymbol{\nabla}p_i + \mu\nabla^2\mathbf{u}_i, \tag{8}$$

where $i = a,\ v$ distinguishes between the arterioles and venules. Fluid flows from the arterioles into the capillary bed (and from the capillary bed into the venules) due to a pressure drop across the vascular tree. Therefore, on the boundaries of the arterioles and porous tissue matrix, and the venules and porous tissue matrix, we impose the boundary conditions

$$\mathbf{u}_a\cdot\mathbf{n}_a = \mathbf{u}_c\cdot\mathbf{n}_a = L_a\left(p_a - p_c\right), \quad \mathbf{u}_v\cdot\mathbf{n}_v = \mathbf{u}_c\cdot\mathbf{n}_v = L_v\left(p_v - p_c\right), \tag{9}$$

respectively, where L_a and L_v represent the 'leakage' of fluid from the arterioles into the porous tissue matrix, and from the porous tissue matrix into the venules, respectively, and $\mathbf{n}_a$, $\mathbf{n}_v$ are the unit outward pointing normals to the arteriole and venule boundaries, respectively. Finally, to close the model, we impose no slip on the arteriole/porous tissue matrix and venule/porous tissue matrix boundaries, so that $\mathbf{u}_a\cdot\boldsymbol{\tau}_a = 0$ and $\mathbf{u}_v\cdot\boldsymbol{\tau}_v = 0$ on the appropriate

boundaries, where $\boldsymbol{\tau}_a$, $\boldsymbol{\tau}_v$ are the unit tangential vectors to the arteriole and venule boundaries.

2.1.4 Parameter Estimation

Geometrical Parameters A representative mean inter- arteriole/venule distance is $10^3\,\mu$m, and the typical size of a dorsal skinfold chamber is 1 cm. This gives a typical value of $\eta = s/L$ of 10^{-1}, justifying the assumption $\eta \ll 1$.

Physiological Parameters There are two key physiological parameters that are not measured experimentally, to the best of our knowledge; these are L_a and L_v, which represent the 'leakage' of fluid from the arterioles into the porous tissue matrix, and from the porous tissue matrix into the venules, respectively. We define dimensionless parameters R_a and R_v that capture these leakage factors and are defined by $R_a = \mu L_a L^4/s^5$, $R_v = \mu L_v L^4/s^5$. Finally, to complete the homogenization process we must relate the magnitude of the blood velocity in the capillaries to that in the arterioles or venules. If V is a typical blood velocity in the arterioles or venules, then V is certainly larger than U. We let the ratio V/U be of size $1/\eta$ (which is large, as $\eta \ll 1$), so that $V/U = V^\star/\eta$, where $V^\star = s^4/d^2L^2 \approx 4$.

2.1.5 Fluid Transport on the Chamber-Scale

Finally, we homogenize from the arteriole/ venule-scale to the chamber length scale to derive the effective model on the length scale of the chamber. The steps here are analogous to those detailed in [23, 22], and also comprise the counterpart to those steps described in Section 2.1.3 for averaging from the micro- to the arteriole/venule scale. This process yields the following model for pressure in the arterioles, venules, capillaries and interstitium,

$$\boldsymbol{\nabla}\cdot(\mathbf{K}_a\cdot\boldsymbol{\nabla}p_a) = \frac{\eta R_a S_a s}{V_a}(p_a - p_c)\,, \quad \boldsymbol{\nabla}\cdot(\mathbf{K}_v\cdot\boldsymbol{\nabla}p_v) = \frac{\eta R_v S_v s}{V_v}(p_v - p_c)\,, \tag{10}$$

$$\boldsymbol{\nabla}\cdot(\mathbf{F}\cdot\boldsymbol{\nabla}p_c) = \frac{R_a S_a s}{V_p}(p_c - p_a) + \frac{R_v S_v s}{V_p}(p_c - p_v)\,, \quad p_t = p_c, \tag{11}$$

where the fluid velocities are given by

$$\mathbf{u}_a = -\frac{1}{\mu}\mathbf{K}_a\cdot\boldsymbol{\nabla}p_a, \quad \mathbf{u}_v = -\frac{1}{\mu}\mathbf{K}_v\cdot\boldsymbol{\nabla}p_v, \quad \mathbf{u}_c = -\frac{\eta}{\mu}\mathbf{F}\cdot\boldsymbol{\nabla}p_c, \quad \mathbf{u}_t = -\frac{\nu\eta^2}{\mu}\mathbf{E}\cdot\boldsymbol{\nabla}p_t. \tag{12}$$

On this length scale of the chamber, the arterioles, venules, capillary bed and interstitium behave as porous media, with coupled flow between the four. As described above, S_a/V_a is the ratio of arteriole surface area to its volume, S_v/V_v is the ratio of the venule surface area to its volume, S_a/V_p is the ratio of arteriole surface area to porous tissue volume, and S_v/V_p is the ratio of venule surface area to porous tissue volume. The parameters R_a and R_v are dimensionless and represent the 'leakage' of fluid from the arterioles into the porous tissue matrix, and from the porous tissue matrix into the venules, respectively. All parameters are defined in Table 1. The fluid permeability tensors $\mathbf{K}_a$, $\mathbf{K}_v$ and $\mathbf{F}$ for the arterioles, venules and capillaries, respectively, on the length scale of the chamber are given in terms of three cell

problems as defined next.

Permeability Tensors for the Interstitial and Capillary Domains

The fluid permeability tensors $\mathbf{E}$ and $\mathbf{K}$ associated with the interstitial and capillary domains are given by

$$\mathrm{E}_{ij} = \delta_{ij} + \frac{1}{V_t}\int_{\text{capillary boundary}} P_t^j n_i \,\mathrm{d}S \quad , \quad \mathrm{K}_{ij} = \frac{1}{V_c}\int_{V_c} w_{ci}^j \,\mathrm{d}V, \tag{13}$$

where P_t^j and $w_{c,i}^j$ solve the cell problems

$$\nabla^2 P_t^j = 0 \text{ in the interstitium}, \quad \mathbf{n}\cdot\boldsymbol{\nabla} P_t^j = \mathbf{n}\cdot\mathbf{e}_j \text{ on the capillary walls}, \tag{14}$$

and

$$\boldsymbol{\nabla}\cdot\mathbf{w}_c^j = 0, \quad \boldsymbol{\nabla} P_c^j = \nabla_X^2 \mathbf{w}_c^j + \mathbf{e}_j \text{ in the capillaries}, \, \mathbf{n}\cdot\mathbf{w}_c^j = 0, \quad \mathbf{w}_c^j\cdot\boldsymbol{\tau} = 0 \,\text{on the capillary walls}. \tag{15}$$

Permeability Tensors Associated with the Arteriolar and Venular Domains

The fluid permeability tensors $\mathbf{F}$, $\mathbf{K}^a$, $\mathbf{K}^v$ are given by

$$\mathrm{F}_{kj} = \left[\delta_{ik} + \frac{1}{V_p}\int_{\text{porous matrix boundary}} P_p^k n_i \,\mathrm{d}S\right] K_{ij}, \quad \mathrm{K}_{ij}^a = \frac{1}{V_a}\iiint_{V_a} w_{a,i}^j \,\mathrm{d}V\,, \quad \mathrm{K}_{ij}^v = \frac{1}{V_v}\iiint_{V_v} w_{v,i}^j \,\mathrm{d}V\,. \tag{16}$$

The vector $\mathbf{P}_p$ solves the cell problem

$$\boldsymbol{\nabla}\cdot\left(\mathbf{K}\cdot\boldsymbol{\nabla} P_p^k\right) = 0, \tag{17}$$

in the porous matrix of the arteriole/venule-scale, with

$$\left(\mathbf{K}\cdot\boldsymbol{\nabla} P_p^k\right)\cdot\mathbf{n}_i = -\mathbf{K}^T\cdot\mathbf{n}_i, \tag{18}$$

for $i = a, v$ on the arteriole/porous matrix and venule/porous matrix boundaries. Additionally, $\mathbf{P}_p$ must be periodic and satisfy the uniqueness condition

$$\iiint_{V_p} \mathbf{P}_p \,\mathrm{d}V = 0. \tag{19}$$

Finally, $\mathbf{w}_a^j$ and $\mathbf{w}_b^j$ are solutions of the cell problem,

$$\boldsymbol{\nabla}\cdot\mathbf{w}^j = 0, \quad \boldsymbol{\nabla} P^j = \nabla^2\mathbf{w}^j + \mathbf{e}_j, \text{ in the arterioles/venules with } \mathbf{n}_i\cdot\mathbf{w}^j = 0, \quad \mathbf{w}^j\cdot\boldsymbol{\tau}_i = 0 \,\text{on the boundaries}, \tag{20}$$

with $\mathbf{w}^j$ and P^j periodic on the arteriole/venule length scales.

2.1.6 Discussion

The chamber-scale model (10)–(12) assumes that fluid flow on the length scale of the chamber is dominated by the arterioles and venules, followed by the capillaries and interstitium in turn (the fluid velocities in the arterioles and venules are largest, whereas those in the capillaries and interstitium are order η and order $\nu\eta^2$ smaller, respectively). The arteriole and venule pressures are coupled to that in the capillaries; indeed, the arteriole and venule pressure appear as sink terms in the capillary pressure equation (11), whereas the capillary pressure appears as a sink in both the arteriole and venule pressure equations (10). Finally, the capillary and interstitial fluid pressures are indistinguishable on the length scale of the chamber, but their associated velocities differ due to the different permeability tensors for transport through the capillary bed and interstitium.

The permeability tensors $\mathbf{K}_a$, $\mathbf{K}_v$, $\mathbf{F}$ and $\mathbf{E}$ can be determined by either comparing predictions of the model (10)–(12) to medical imaging data, or by solving explicitly the four unit cell problems (13)–(20) that must be solved on the length scale of the arterioles, venules and capillaries, once the geometry of these networks has been specified. Essentially, the calculation of $\mathbf{K}_a$, $\mathbf{K}_v$, $\mathbf{F}$ and $\mathbf{E}$ involves averaging the counterpart local flow variations over their representative unit cell.

We employ this model to investigate the key architectural and functional features that influence fluid perfusion in the capillaries, in a case study relating to a simplified representation of a dorsal skinfold chamber. To simplify the model to one which is sufficiently computationally tractable to explore the impact of key vascular parameters on the model predictions, first of all we assume that the arteriole and venule networks have identical topological and physiological properties (*i.e.* $\mathbf{K}_a = \mathbf{K}_v$, $S_a = S_v$, $V_a = V_v$ and $R_a = R_v$), and that all networks are isotropic so that permeability tensors are proportional to the identity matrix. Specifically we let $\mathbf{K}_a = \mathbf{K}_v = h\mathbf{I}$, $\mathbf{F} = (k/V^\star)\,\mathbf{I}$, and $\mathbf{E} = \left(\kappa s^2/V^\star\right)\mathbf{I}$. Here $V^\star = \eta^2/\nu^2$ relates the magnitude of the blood velocity in the capillaries to that in the arterioles or venules (specifically if V is a typical blood velocity in the arterioles or venules, and U is a typical capillary blood velocity, then $V/U = V^\star/\eta$), and $\kappa = k^{int}s/d^3$ is the dimensionless interstitial permeability on the length-scale of the capillaries. These relationships are a direct consequence of the homogenization approach. Now the pressure and velocity equations can be written in terms of parameters that depend purely on the arteriole and venule network, and those that depend on the capillary network properties,

$$\nabla^2 p_a = \frac{\eta r}{hn}\left(p_a - p_c\right), \quad \nabla^2 p_v = \frac{\eta r}{hn}\left(p_v - p_c\right), \quad \nabla^2 p_c = \frac{r}{P}\left(2p_c - p_a - p_v\right), \quad p_t = p_c, \tag{21}$$

and

$$\mathbf{u}_a = -\frac{h}{\mu}\boldsymbol{\nabla} p_a, \quad \mathbf{u}_v = -\frac{h}{\mu}\boldsymbol{\nabla} p_v, \quad \mathbf{u}_c = -\frac{\eta P}{\mu}\boldsymbol{\nabla} p_c, \quad \mathbf{u}_t = -\frac{\eta^2 C}{\mu}\boldsymbol{\nabla} p_t. \tag{22}$$

Here, n and r depend purely on the arteriole and venule network properties; n is the volume ratio of arterioles (or venules), as a proportion of the volume of the porous tissue, $n = V_a/V_p = V_v/V_p$, whilst r depends on the arteriole and

venule length scale, s, and the chamber length scale, L, together with the geometrical and physiological properties of the arteriole and venule networks, through $r = R_a s S_a / V_p = R_v s S_v / V_p$.

The parameter $C = k^{int} L^2 / s^2$ depends on the arteriole and venule length scale, s, and chamber length scale, L, together the with permeability of the interstitium, k^{int}. Finally, $P = k\nu^2/\eta^2$ is the key parameter that depends on the capillary permeability, k, and capillary length scale, d (note that varying d is equivalent to changing the density of the capillary network). The parameter P is a measure of the capillary permeability, multiplied by the ratio of the capillary to arteriole with respect to the arteriole to tumour length scales.

2.2 Drug Transport Model

We denote the drug concentration by c, with subscripts a, v, c and t denoting the arterioles, venules, capillaries and interstitium, respectively. Here we focus on vinblastine, a widely used cell-cycle specific chemotherapy drug for which the transport kinetics were characterised in [36]; however, our models are applicable to any tracer molecule, and can be extended to include different drug kinetics. Vinblastine is advected and diffuses in the arterioles, venules, capillaries and interstitium, and the Péclet number (which represents the ratio of diffusive to convective timescales) is a good way to compare the relative importance of these transport mechanisms. The Péclet number for transport in the capillaries is $Ud/D_c \approx 3.8$, where $U \approx 25\,\mu\text{m s}^{-1}$ is the blood velocity and $D_c \approx 3.3 \times 10^{-6}\,\text{cm}^2\text{s}^{-1}$ is the diffusion coefficient [36]; therefore, advection and diffusion are in balance on the length scale of the capillaries. On the length scale of the chamber, the Péclet number for transport in the capillaries is $UL/D_c \approx 7.6 \times 10^3$ indicating that advection dominates over diffusion. Advection also dominates in the arterioles and venules on the length scale of the chamber.

We describe transport from the vessels into the tissue using a membrane law that relates the jump in concentration flux across the membrane, $[\mathbf{J}\cdot\mathbf{n}]^+_-$ (where $\mathbf{J}$ denotes the concentration flux, $\mathbf{n}$ is the unit outward pointing normal to the vessel / tissue boundary, and '$-$' and '$+$' denote either side of this boundary), to the concentration jump across it, $[c]^+_-$, via $[\mathbf{J}\cdot\mathbf{n}]^+_- = r\,[c]^+_-$, where r is the boundary permeability (units cm s^{-1}) [10]. To give an example, we describe drug transport on the micro-scale by

$$\frac{\partial c}{\partial t} + (\mathbf{u}\cdot\boldsymbol{\nabla})\,c = D\nabla^2 c, \tag{23}$$

where D takes the value D_c within the capillary domain, and D_t within the interstitial domain, with

$$(c_c\mathbf{u}_c - D_c\boldsymbol{\nabla}c_c)\cdot\mathbf{n} - (c_t\mathbf{u}_t - D_t\boldsymbol{\nabla}c_t)\cdot\mathbf{n} = r\,(c_c - c_t)\,, \quad \text{on the capillary walls,} \tag{24}$$

subject to an initial condition on the drug concentration field. As for the fluid transport problem reported in Section 2.1, we proceed by first homogenizing from the micro- to the arteriole/venule-scale, and then to the chamber-scale to derive an effective model for drug transport. Full details of this process are not reported for succinctness, but also

closely follow the approaches in [23, 22]. The key steps involve (for the example of homogenizing from the micro- to the arteriole/venule-scale): (a) assuming length scale separation so that $\boldsymbol{\nabla} = \boldsymbol{\nabla}_{\text{micro}} + \nu\boldsymbol{\nabla}_{\text{arteriole/venule}}$ in equations (23–24), (b) move onto the timescale for advection on the arteriole/venule length scale by rescaling $t = t/\nu$, (c)expanding all variables asymptotically in powers of ν, (c) equating coefficients of powers of ν in (23)–(24), averaging over the micro-scale to derive the arteriole/ venule-scale relationships.

This process determines the following transport model for vinblastine on the chamber-scale are

$$\frac{\partial c_a}{\partial t} + \boldsymbol{\nabla}\cdot(c_a\mathbf{u}_a) = -\frac{S_a T_a}{V_a}(c_a - c_c), \quad \frac{\partial c_v}{\partial t} + \boldsymbol{\nabla}\cdot(c_v\mathbf{u}_v) = -\frac{S_v T_v}{V_v}(c_v - c_c), \tag{25}$$

$$\frac{\partial c_c}{\partial t} + \boldsymbol{\nabla}\cdot(c_c\mathbf{u}_c) = \frac{S_a T_a}{V_p}(c_a - c_c) + \frac{S_v T_v}{V_p}(c_v - c_c), \tag{26}$$

where the fluid velocities $\mathbf{u}_a$, $\mathbf{u}_v$ and $\mathbf{u}_c$ are given by (22), and T_i for $i = a, v$ are coefficients given by $T_a = r_a/\eta^2$, $T_v = r_v/\eta^2$ that represent drug transport from the arterioles (or venules) into the porous tissue matrix comprised of capillaries and interstitium. The drug concentration in the interstitium and capillaries are indistinguishable on the chamber scale so that $c_t = c_c$. This is a direct consequence of the fact that (a) advection and diffusion of vinblastine are balanced in the capillaries and interstitium (the concentration of vinblastine is well-mixed over the distances relevant here) and (b) vinblastine is a tracer, so there is no uptake to introduce spatial gradients in concentrations.

3 Fluid Transport Results

We investigate the impact of varying the properties of the capillary bed on fluid perfusion in a case study of a simplified geometry representative of a dorsal skinfold chamber, by solving the fluid transport equations (21)–(22) using the finite element package COMSOL Multiphysics. To achieve this, we fix the geometry of the chamber, the topology and physiological properties of the arteriole and venule networks (*i.e.* the parameters n and r), and the interstitial permeability (*i.e.* the parameter C), and test the impact of varying the capillary configuration which explicitly means varying the parameter P.

Experimentally chambers are imaged in 2D slices through their centre, so we simplify the investigation by assuming a 2D setup. The chamber is represented in 2D by a square of dimensions L cm $\times L$ cm with a central circle of cancerous tissue (region 1), as depicted in Figure 6. A source artery and sink vein are seeded in region 1, and are represented by a circle, where the upper half-circle is the artery, and the lower half-circle is the vein (this mimics the typical experimental scenario where the tumour mass is connected to the host blood supply through seed ing an artery and vein into the region). The remainder of the chamber is comprised of malignant tissue (region 2). Throughout the chamber we solve equations (21) for the arteriole and venule pressures; we impose a pressure drop across the vasculature by applying $p_a = 50$ mmHg on the artery boundary and $p_v = 10$ mmHg on the vein boundary. We also apply no flux of p_a and p_v across the outer boundary of the chamber, and no flux jump across the interface between regions 1 and 2. In region

2, we fix the value of P at $P_2 = k_2 L^2 d_2^2/s^4$. We impose no flux of p_c through the outer boundary of the chamber, and no flux jump across any internal boundaries. Finally, for simplicity, we assume that the arteriole, venule and capillary networks in region 2 each have a hexagonal structure, as shown in Figure 8 (b). This allows us to test the perfusion sensitivity in response to variation in the capillary structure in region 1. Table 1 provides a summary of the fixed parameters.

To test the impact of varying P on fluid perfusion in the capillaries and interstitium, we evaluate the flux of fluid in the capillaries and interstitium that travels from region 1 into region 2,

$$Q_c = \int \mathbf{u}_c \cdot \mathbf{n} \, \mathrm{d}S = -\frac{\eta}{\mu} P \int_\Gamma \boldsymbol{\nabla} p_c \cdot \mathbf{n} \, \mathrm{d}S, \quad Q_t = \int \mathbf{u}_t \cdot \mathbf{n} \, \mathrm{d}S = -\frac{\eta^2 C}{\mu} \int_\Gamma \boldsymbol{\nabla} p_t \cdot \mathbf{n} \, \mathrm{d}S = \frac{\eta C}{P} Q_c, \tag{27}$$

where Γ is the interface between both regions and $\mathbf{n}$ is the unit outward pointing normal to Γ.

The results presented here are for a fixed value of $R_a = R_v = 10^{-2}$. These parameters characterise the leakage of fluid from the arterioles and venules into the capillary bed and are not measured experimentally. Model outcomes are only sensitive to the value of $R_a = R_v$ when this leakage coefficient is small (representing the physiologically unrealistic situation of the arterioles and venules short-circuiting the capillary bed). Otherwise, model predictions are much more sensitive to the value of P which captures the capillary bed properties.

Figure 5 shows how the fluxes Q_c and Q_t vary as a consequence of changes in the permeability and density of the region 1 capillary network (through P). For the smallest value of P tested ($P = 10^{-16}\,\mathrm{m}^2$), Q_c and Q_t are small and positive, corresponding to a net flux of fluid from region 1 to region 2. As P increases, so do Q_c and Q_t until maxima are reached when $P \approx 1.25 \times 10^{-12}\,\mathrm{m}^2$ (here $Q_c = 1.45 \times 10^4\,\mu\mathrm{m}^2\,\mathrm{s}^{-1}$ and $Q_t = 6.18 \times 10^3\,\mu\mathrm{m}^2\,\mathrm{s}^{-1}$, respectively). As P now increases from $1.25 \times 10^{-12}\,\mathrm{m}^2$, Q_c and Q_t decrease and are negative for $P > 5.2 \times 10^{-6}\,\mathrm{m}^2$, corresponding to a net flux of fluid from region 2 to region 1.

Figures 6 show the arteriole and venule fluid pressures throughout the chamber for an example value $P = 10^{-14}\,\mathrm{m}^2$. Given that the arteriole and venule properties are fixed, arteriole and venule pressure distributions is similar for all values of P; however, the precise pressure drop across the arteriole and venous networks does vary as the underlying capillary bed properties are varied (results not shown).

Figure 7 (a) shows the capillary pressure distribution when $P = 10^{-14}\,\mathrm{m}^2$. This low value of P corresponds to either a low capillary network permeability, k, or high density (through the capillary length scale d) in region 2. The capillary pressure is highest (or lowest) in the immediate vicinity of the source artery (or sink vein), but decays relatively quickly to a background value of around 31 mmHg. Indeed, the capillary pressure in most of the chamber is approximately constant. This results in gradients in p_c from the immediate vicinity of the source artery/sink vein, and the consequent positive values of Q_c and Q_t at this value of P.

Figure 7 (b) shows the pressure distribution for $P = 1.25 \times 10^{-12}\,\mathrm{m}^2$, corresponding to the maxima of Q_c and Q_t

(see Figure 5). The spatial gradients in the capillary pressure throughout the chamber are larger, resulting in larger capillary and interstitial fluid velocities, and the consequent high values of Q_c and Q_t. This increase in P relative to Figure 7a could be achieved by either increasing the permeability of the region 1 capillary network, or decreasing its density.

As P increases from $1.25 \times 10^{-12}\,\mathrm{m}^2$, Q_c and Q_t progressively decrease and are negative for $P > 5.2 \times 10^{-12}\,\mathrm{m}^2$, corresponding to a net flux of fluid from region 2 to region 1. The consequence of increasing P (from $1.25 \times 10^{-12}\,\mathrm{m}^2$) on the pressure distributions can be seen in Figures 7 (c)–(e). As a result of the asymmetrical position of the seeded artery and vein (and the value of P relative to $P_2 = 9.36 \times 10^{-12}\,\mathrm{m}^2$), as P increases a localised region of high/low capillary pressure develops in the top/bottom left hand corner of the chamber, and the capillary pressure in region 1 approaches constant. Therefore, although there is a net flow from the region 2 to region 1, the capillary and interstitial fluid velocities within region 1 become very small, and drugs will accumulate in the tumour periphery as opposed to being transported throughout the tumour.

Larger capillary and interstitial velocities in region 2 are beneficial to distribute drugs by advection to the cancerous cells. This analysis indicates that an optimal P-value of $1.25 \times 10^{-12}\,\mathrm{m}^2$ will achieve this, and can be realized by varying the permeability or density of the capillary bed. For example, if the P-value of region 1 is larger than $1.25 \times 10^{-12}\,\mathrm{m}^2$, vascular intervention that reduces the P-value would benefit drug distribution, and could be achieved by either reducing the permeability or increasing the density of the capillary network. Similarly, if $P < 1.25 \times 10^{-12}\,\mathrm{m}^2$, vascular intervention that increases the P-value would benefit drug distribution.

Finally, we investigate some explicit network examples. We test 8 different structures for the region 1 capillary network; the unit cells for these networks are shown in Figure 8. Figures 8 (a) and (b) are two examples of regular networks (a grid and hexagonal structure, motivated by the honeycomb structures imaged in [34]), whereas the remaining 6 structures are more irregular (the networks in Figure 8 (e)–(h) have identical inlets and outlets to the grid network, and are formed by progressively removing one link of the network each time). Figure 9 shows the values of the permeability tensor $\mathbf{F} = F_{ij}$ ($\mu\mathrm{m}^2$) which are determined by solving the full cell problems given in Section 2.1.5 using COMSOL Multiphysics. We assume that the arteriole and venule networks, and the region 2 capillary network, take the hexagonal structure of Figure 8 (b). We also take $d = 50\,\mu\mathrm{m}$ in both regions.

The P-values and corresponding values of Q_c and Q_t for each network are summarized by bar charts in Figures 9. The P–values for these networks lie in the range $9.52 \times 10^{-12}\,\mathrm{m}^2$ to $6.98 \times 10^{-10}\,\mathrm{m}^2$, and increase from smallest to largest in the order Hexagonal, Irregular-II, Irregular-I, Grid, Grid-III, Grid-I, Grid-II, Grid-IV (see Table 2). If we exclude the Hexagonal case, all P-values lie in the range $3.13 \times 10^{-11}\,\mathrm{m}^2$ to $6.98 \times 10^{-10}\,\mathrm{m}^2$, and correspond to virtually constant capillary pressure in region 1. These values are larger than the optimal value of $P = 1.25 \times 10^{-12}\,\mathrm{m}^2$ identified earlier, indicating that vascular intervention to decrease the P-value would benefit anticancer drug distribution throughout region 1. This decrease in P-value could be achieved by either decreasing the permeability of the networks

(*i.e.* decreasing the matrix components F_{ij}), or by increasing the density of the capillary bed by decreasing d.

4 Vinblastine Distribution Results

Vinblastine is a chemotherapeutic drug frequently used to treat various cancers via intravenous delivery. As its properties are well-characterised [18], we next investigate vinblastine perfusion in a dorsal skinfold chamber, by solving the equations for vinblastine transport given by equations (25)–(26) using the finite element package COMSOL Multiphysics. To facilitate the computation, the equations (25)–(26) are solved with an additional numerical diffusion constant of value $\mathcal{O}\left(\eta^2\right)$ in keeping with the next order corrections to the transport model which are neglected. Vinblastine is delivered exclusively intravenously to a patient using either (i) a single injection, or (ii) constant perfusion of the drug to the patient over a long time period. These correspond to two different boundary conditions for the arteriole concentration, c_a, on the artery wall. The functional form for this boundary condition is denoted by σ and discussed in more detail below. On the external boundaries of the chamber, we apply no flux condition for each concentration component, with no flux jump on the internal boundaries.

Treatment Through a Single Injection A dose of drug delivered by injection will be metabolized in the bloodstream as time progresses. For vinblastine this metabolism occurs over four phases [18], namely an initial fast phase which represents the distribution of the blood through the body, and three further slow phases representing the redistribution and metabolism of the drug in different organs of the body. This can be represented mathematically by the function

$$\sigma\left(t\right) = A\mathrm{e}^{-k_1 t} + B\mathrm{e}^{-k_2 t} + C\mathrm{e}^{-k_3 t} + D\mathrm{e}^{-k_4 t}\,, \tag{28}$$

where the k_i $(i = 1, 2, 3, 4)$ represent the half lives of the four separate phases, and A, B, C and D are constants to be determined for a specific individual. The half lives for the four distribution/metabolism phases are 1 sec, 4 sec, 53 sec and 1173 sec respectively, giving $k_1 = 41.6\,\mathrm{min}^{-1}$, $k_2 = 0.17\,\mathrm{min}^{-1}$, $k_3 = 1.3 \times 10^{-2}\,\mathrm{min}^{-1}$, and $k_4 = 5.9 \times 10^{-4}\,\mathrm{min}^{-1}$.

The constants A, B, C, and D are determined from the initial dose, together with three conditions on the level of metabolism after each phase's half life [18]. We consider an initial dose of 2700 nM; for a person of weight 64 kg (and blood volume $\approx$ 4.4 litres) the remaining conditions are $\sigma\left(t = 4\mathrm{min}\right) = 700\,\mathrm{nM}$, $\sigma\left(t = 53\,\mathrm{min}\right) = 150\,\mathrm{nM}$ and $\sigma\left(t = 1173\,\mathrm{min}\right) = 10\,\mathrm{nM}$ which give $A = 1557$ nM, $B = 862$ nM, $C = 261$ nM, and $D = 20$ nM.

Treatment through Constant Perfusion An alternative regime involves maintaining a constant concentration of vinblastine in the bloodstream over a longer time period. To limit damage to the patient, the achievable concentration is lower than the initial injection concentration; indicative values are a concentration of 8nM applied constantly to the patient

over a period of 5 days [3]. The boundary condition on the artery wall is therefore

$$\sigma(t) = \begin{cases} 8\,\text{nM} & \text{for } 0 \le t \le 120 \text{ hours} \\ 0 & \text{for } t > 120 \text{ hours} \end{cases} . \tag{29}$$

Next we solve equations (25)–(26) to test whether treatment through a single injection or constant perfusion is more efficient at killing tumour cells in a dorsal skinfold chamber. To the best of our knowledge there are no data available on r_a and r_v, which represent the timescale for vinblastine transfer between the arterioles and capillary bed, and between the capillary bed and venules. Here we fix $r_a = r_v = 23.1 \times 10^{-12}\,\text{s}^{-1}$ based on our order of magnitude estimates using homogenization theory. Varying $r_a = r_v$ influences the time delay before the maximum value of the capillary/interstitial concentration, together with the values at the peak. It does not, however, alter the qualitative conclusions that will be made.

We evaluate the cell kill rate as a consequence of the vinblastine treatment. The maximum kill rate is $1/24$ hours^{-1} [21], whereas the concentration of vinblastine required to kill cells at the half-maximal kill rate is 2 nM [8]. Finally the cell kill rate is proportional to concentration for low drug concentrations so we assume that the cell-kill rate, $M_c(c_t) = \dfrac{\rho_1 c_t}{\rho_2 + c_t}$ where $\rho_1 = 1/24$ hr^{-1}, $\rho_2 = 2$ nM.

We test the impact of the cell-kill rate on the interstitial volume fraction by modelling the time-dependent changes in this volume fraction using a partial differential equation, where we explicitly focus on the competition between cell proliferation and death, with the latter determined as a function of the local concentration of drug. This serves as a first approximation to the impact of the treatment therapy, as there is no mechanism for volume change due to tumour growth or regression in the models presented here, but provides an illustrative example of the utility of the model. We denote the interstitial volume fraction by ϕ, and capture changes in this volume fraction through

$$\frac{\partial \phi}{\partial t}(\mathbf{x}, t) = K\phi(\mathbf{x}, t) - M_c(c_t(\mathbf{x}, t))\,\phi(\mathbf{x}, t) , \tag{30}$$

subject to the initial condition $\phi(\mathbf{x}, 0) = n_t$, where K is the net cell proliferation rate and depends on the cell line used. We note that equation (30) assumes that the cell proliferation and cell kill rates are proportional to the interstitial volume fraction, following similar approaches in the literature. Finally we assess cell kill by evaluating the spatial average of ϕ, given by

$$\phi^{av}(t) = \frac{1}{\text{Area of Region 1}} \int_{\text{Region 1}} \phi(\mathbf{x}, t)\, \text{d}V, \tag{31}$$

where the area of the region 1 is 0.4948 cm^2 for the simulations in this paper. We present results for three cases of the cell proliferation rate $K = 1/29,\ 1/31,\ 1/33$ hours^{-1}.

The individual average vinblastine concentrations in the arterioles, venules, capillaries and interstitium are shown in Figures 11, 12. For both treatment through injection or constant perfusion the concentrations in the arterioles closely

mimic the treatment profile. Variation due to the capillary structure in region 1 is barely detectable as the timescale for vinblastine transport is much faster than that for uptake or proliferation. Indeed for constant perfusion the vinblastine concentration is constant (to 3 significant figures) across the entire chamber within 3.5 hours (the simulation length is 712 hours).

The value of ϕ^{av} increases and decreases from the initial value due the balance of cell kill and proliferation, as described by equations (30)–(31). Given that the concentration of vinblastine is uniform throughout the chamber after about 3.5 hours, the only dependence of ϕ^{av} on vascular structure occurs through the initial condition $\phi(\mathbf{x}, 0) = n_t$. A comparison of treatment through single injection and constant perfusion is shown in Figure 10 for three different cases of the cell proliferation rate $K = 1/29,\ 1/31,\ 1/33$ hours^{-1}. The concentration of vinblastine delivered to the chamber is much lower for constant perfusion than for a single injection, but is maintained for a longer period of time. This does not appear to have a significant cumulative effect. For example when the rate of cell proliferation $K = 1/29$ hours^{-1}, the final values of ϕ^{av} were in the range $(1.4936, 2.0616)$ for a single injection, and the range $(9.2587, 12.7797)$ for constant perfusion. This pattern of behaviour is replicated for other values of the rate of cell proliferation, K.

The modelling outputs can also predict the timing of a second injection of vinblastine. This decision could be made based on various criteria such as when the value of ϕ^{av} reaches a minimum value, or when the vinblastine concentration in the capillaries drops to a prescribed value. For example, when the cell proliferation rate $K = 1/31$ hours^{-1} the minimum value of ϕ^{av} is achieved after 14.8 days and could motivate a two-week cycle of vinblastine treatment. We note that this framework neglects multiple features necessary to quantitatively predict drug treatment efficacy (for example, tumour growth, toxicity, etc); however, this case study does enable the behaviour of the new four-compartment model to be explored. We also note that a much more marked dependence on vascular architecture would be expected for drugs which decay and are metabolised, due to the impact of spatial gradients in the drug profile at the scale of the capillaries.

5 Conclusions

We have presented a new four-component model to investigate fluid and vinblastine perfusion in a dorsal skinfold chamber. The model incorporated arteriole, capillary, and venule networks, together with the interstitium, and provides a framework for incorporating the impact of these hierarchical structures on fluid and drug perfusion to tumours. The impact of treatment through a single injection and through constant perfusion were tested, and the dependence of both the fluid and vinblastine perfusion results on the vascular network were highlighted.

The multiscale model of blood transport was used to identify a single parameter (P in this paper) which relates chamber-scale fluid perfusion to the capillary bed properties (specifically the permeability and density of the capillary network). By fixing the topological and physiological properties of the arteriole and venules networks, a P-value of $1.25 \times 10^{-12}\,\mathrm{m}^2$ was identified that maximises fluid perfusion through the tumour region of the chamber.

The multiscale model of vinblastine transport was used to explore the effectiveness of treatment via a single injection or constant perfusion of the drug, when the cancer cell proliferation rate in chamber was $K = 1/29, 1/31, 1/33\,\text{hours}^{-1}$. In each case, treatment through injection was significantly more effective than that through constant perfusion, although we note the necessity for more complexity to be incorporated, and model validation, before these predictions could be taken forward. In addition, it was demonstrated how to use the model outputs to predict when to deliver a second course of chemotherapy.

There are numerous opportunities for further extension of the approach in this paper, spanning incorporating more complexity into the modelling frameworks, and validation of the model predictions again real world data. The current work focuses on the development of a new four-component model that incorporates relevant transport information on a hierarchy of length scales, and its implementation in a case study to explore fluid and drug perfusion in a relevant experimental setup. Further opportunities for model development include extension to realistic, 3D vascular geometries and tumour architectures acquired using medical imaging, including more realistic haemodynamic descriptions at the capillary scale, the incorporation of more sophisticated drug kinetics (for example decay and metabolism, which will involve a different homogenised model), and also tumour growth. There is an outstanding need for more sophisticated descriptions of tumour perfusion, growth and response to treatment to inform therapy developments for cancer. This would require extensive validation of the assumptions and predictions of the model against measurable data. We leave these as important next steps to develop the utility of this approach in informing tumour treatment strategies.

Acknowledgments RJS and PWS acknowledge funding from Rosetrees Trust (M135-F1 and M601). TR acknowledges the award of a Royal Society University Research Fellowship.

Declarations of Interest None.

Glossary of Terms

Symbol	Definition	Units
Dimensional Parameters		
d	Inter-capillary separation	μm
s	Inter-arteriole and inter-venule separations	μm
L	Chamber length scale	cm
$\mathbf{u}$	Fluid velocity	cm s^{-1}
p	Fluid pressure	mmHg
$\mathbf{K}_a$ and $\mathbf{K}_v$	Arteriole and venule fluid permeability tensors	m^2
$\mathbf{F}$ and $\mathbf{E}$	Capillary and interstitial fluid permeability tensors	m^2
S_a and S_v	Arteriole and venule surfaces areas in contact with porous tissue matrix	m^2
V_a, V_v and V_p	Arteriole, venule and porous tissue matrix volumes	m^3
μ	Viscosity of blood	Pa s
h	Isotropic component of arteriole and venule permeability tensors	m^2
k	Isotropic component of capillary permeability tensor	m^2
k^{int}	Interstitial permeability	m^2
$P = k\nu^2/\eta^2$	Parameter that captures the region 2 capillary network properties	m^2
$C = k^{int}/\eta^2$	Parameter that captures the interstitial permeability	m^2
c	Vinblastine concentration	nM
U	Typical capillary velocity	$\mu\text{m}\,\text{s}^{-1}$
D_c	Vinblastine diffusivity in the capillaries	$\text{cm}^2\,\text{s}^{-1}$
r	Membrane permeability to vinblastine transport	s^{-1}
$T_a = r_a/\eta^2$	Parameter representing drug transport from the arterioles into the porous tissue matrix	s^{-1}
$T_v = r_v/\eta^2$	Parameter representing drug transport from the arterioles into the porous tissue matrix	s^{-1}
Q_c	Flux of fluid in the capillaries from region 1 to region 2	$\mu\text{m}^2\,\text{s}^{-1}$
Q_t	Flux of fluid in the interstitium from region 1 to region 2	$\mu\text{m}^2\,\text{s}^{-1}$
$\sigma\,(t)$	Vinblastine treatment boundary condition on the artery wall	nM
M_c	Functional form for cell kill rate due to vinblastine	nM hr^{-1}
K	Net cell proliferation rate	s^{-1}
Dimensionless Ratios		
$\nu = d/s$	Ratio of capillary to arteriole/venule length scales	-
$\eta = s/L$	Ratio of arteriole/venule to chamber length scales	-
R_a and R_v	Dimensionless parameters that represent fluid 'leakage' from the arterioles and venules into the porous tissue matrix	-

$n = V_a/V_p = V_v/V_p$	Volume ratio of arterioles (and venules) as a proportion of the volume of the porous tissue	-
$r = R_a s S_a/V_p = R_v s S_v/V_p$	Dimensionless parameter that depends on the geometrical and physiological properties of the arteriole and venule networks	-
n_a	Volume fraction of arterioles	-
n_v	Volume fraction of venules	-
n_p	Volume fraction of porous tissue matrix	-
n_c	Volume fraction of capillaries	-
n_t	Volume fraction of interstitium	-
$\phi(\mathbf{x}, t)$	Interstitial volume fraction	-
$\phi(t)^{av}$	Volume-averaged interstitial volume fraction	-

References

[1] J. Baish, Y. Gazit, D. Berk, M. Nozue, L. Baxter, and R. Jain, *A novel approach to examine the role of vascular heterogeneity in nutrient and drug delivery for tumors: An invasion percolation model*, Microvascular Research, 51 (1996), pp. 327–246.

[2] S. J. Chapman, R. J. Shipley, and R. Jawad, *Multiscale modeling of fluid transport in tumors*, Bull. Math. Biol., 70:8 (2008), pp. 2334–2357.

[3] C. Chong, C. Logothetis, N. Savaraj, H. A. Fritsche, A. Gietner, and M. Samuels, *The correlation of vinblastine pharmacokinetics to toxicity in testicular cancer patients.*, Journal of Clinical Pharmacology, 28 (August 1988), pp. 714–718.

[4] L. J. Cooper, K. R. Daly, P. D. Hallett, M. Naveed, N. Koebernick, A. G. Bengough, T. S. George and T. Roose, *Fluid flow in porous media using image-based modelling to parametrize Richards' equation*, Proc. R. Soc. A, 473 (2017), pp. 20170178.

[5] K. R. Daly and T. Roose, *Determination of macro-scale soil properties from pore-scale structures: model derivation*, Proc. R. Soc. A, 474 (2018), pp. 20170141.

[6] H. Darcy, *Les fontaines publiques de la ville de Dijon*, Dalmont, Paris, 647 (1856).

[7] A. d'Esposito, P.W. Sweeney, M. Ali, M. Saleh, R. Ramasawmy, T.A. Roberts, G. Agliardi, A. Desjardins, M.F. Lythgoe, R.B. Pedley, R.J. Shipley and S. Walker-Samuel, *Computational fluid dynamics with imaging of cleared tissue and of in vivo perfusion predicts drug uptake and treatment responses in tumours*, Nat. Bio. Med., 2(10) (2018), pp.773–787.

[8] M. Hall, C. Martin, D. Ferguson, R. M. Phillips, T. Hambley, and R. Callaghan, *Comparative efficacy of novel platinum(IV) compounds with established chemotherapeutic drugs in solid tumour models*, Biochemical Pharmacology, 67 (January 2004), pp. 17–30.

[9] U. Hornung, *Homogenization and porous media*, New York, USA: Springer, 1997.

[10] R.K. Jain, *Transport of molecules across tumor vasculature*, Cancer and Metastasis Reviews, 6 (1987), pp. 559–593.

[11] R.K. Jain, *Barriers to drug delivery in solid tumours*, Sci Amer, 271 (1994), pp. 59–65.

[12] M. Konerding, E. Fait, and A. Gaumann, *3D microvascular architecture of pre-cancerous lesions and invasive carcinomas of the colon.*, British Journal of Cancer, 84 (2001), pp. 1354–62.

[13] H. Lehr, A. Guhlmann, D. Nolte, D. Keppler, and K. Messmer, *Leukotrienes as mediators in ischemia-reperfusion injury in a microcirculation model in the hamster*, J Clin Invest, 87 (1991), pp. 2036–2041.

[14] H.-A. Lehr, M. Leunig, M. Menger, D. Nolte, and K. Messmer, *Dorsal skinfold chamber technique for intravital microscopy in nude mice*, American Journal of Pathology, 143 (October 1993), pp. 1055–1062.

[15] S. Modok, P. Hyde, H. Mellor, T. Roose, and R. Callaghan, *Diffusivity and distribution of vinblastine in three-dimensional tumour tissue: Experimental and mathematical modelling*, European Journal of Cancer, 42 (2006), pp. 2404–2413.

[16] B.A. Warren, *The vascular morphology of tumors*, Tumor Blood Circulation: Angiogenesis, Vascular Morphology and Blood Flow of Experimental and Human Tumors, Peterson, H-I (ed) (1979), pp. 1–47.

[17] J.A. Nagy, S-H. Chang, A.M. Dvorak and H.F. Dvorak, *Why are tumour blood vessels abnormal and why is it important to know?*, British Journal of Cancer, 100 (2009), pp. 865–869.

[18] R. Owellen, C. Hartke, and F. Hains, *Pharmacokinetics and metabolism of vinblastine in humans.*, Cancer Research, 37 (Summer 1977), pp. 2597–2602.

[19] G. Pavliotis and A. Stuart, *Multiscale Methods: Averaging and Homogenization*, New York, USA: Springer, 2008.

[20] A. Pries, A. Cornelissen, A. Sloot, M. Hinkeldey, M. Dreher, M. Hopfner, M. Dewhirst, and T. Secomb, *Structural adaptation and heterogeneity of normal and tumor microvascular networks*, PLoS Comput. Biol., 5 (2009).

[21] A. Saraste, *Morphologic criteria and detection of apoptosis.*, Herz, 24 (May 1999).

[22] R. J. Shipley, *Multiscale Modelling of Fluid and Drug Transport in Vascular Tumours*, PhD thesis, University of Oxford, 2008.

[23] R. J. Shipley and S. J. Chapman, *Multiscale modelling of fluid and drug transport in vascular tumours*, Bulletin of Mathematical Biology, 72:6 (2010), pp. 1464–1491.

[24] R.J. Shipley, A. Smith, P.W. Sweeney, A.R. Pries, T.W. Secomb, *A hybrid discrete-continuum approach for modelling microcirculatory blood flow*, Mathematical Medicine and Biology: A Journal of the IMA, dqz006 (2019), pp. 1-18.

[25] P. W. Sweeney, A. d'Esposito, S. Walker-Samuel and R. J. Shipley, *Modelling the transport of fluid through heterogeneous, whole tumours in silico*, PLoS Comput Biol, 15:6 (2019), pp. e1006751.

[26] R. Tong, Y. Boucher, S. Kozin, F. Winkler, D. Hicklin, and R. Jain, *Vascular normalization by vascular endothelial growth factor receptor 2 blockade induces a pressure gradient across the vasculature and improves drug penetration in tumors*, Cancer Res, 64 (2004), pp. 553–563.

[27] L. Baxter and R. Jain, *Transport of fluid and macromolecules in tumors I. Role of interstitial pressure and convection*, Microvascular Research, 37 (1989), pp. 77–104.

[28] L. Baxter and R. Jain, *Transport of fluid and macromolecules in tumors II. Role of heterogeneous perfusion and lymphatics*, Microvascular Research, 40 (1990), pp. 246–263.

[29] R. Fåhraeus, *Die strölmungsverhältnisse und die verteilung der blutzellen im gefäbsystem. Zur frage der bedeutung der intravasculären erythrocytenaggregation*, Klinische Wochenschrift, 7 (1928), pp. 100–106.

[30] R. Fåhraeus and T. Lindqvist, *The viscosity of the blood in narrow capillary tubes*, Am. J. Physiol., 96 (1931), pp. 562–568.

[31] A. Guyton, H. Granger, and A. Taylor, *Interstitial fluid pressure*, Physiological Reviews, 51 (1971), pp. 527–563.

[32] R. Jain, R. Tong, and L. Munn, *Effect of Vascular Normalization by Antiangiogenic Therapy on Interstitial Hypertension, Peritumor Edema, and Lymphatic Metastasis: Insights from a Mathematical Model*, Cancer Research, 67 (2007), p. 2729.

[33] T. Kenner, *The measurement of blood density and its meaning*, Basic Research in Cardiology, 84 (1989), pp. 111–124.

[34] M. Konerding, E. Fait, and A. Gaumann, *3D microvascular architecture of pre-cancerous lesions and invasive carcinomas of the colon.*, British Journal of Cancer, 84 (2001), pp. 1354–62.

[35] M. Konerding, W. Maikusch, B. Klapthor, C. Van Ackern, E. Fait, S. Hill, C. Parkins, D. Chaplin, M. Presta, and J. Denekamp, *Evidence for characteristic vascular patterns in solid tumours: Quantitative studies using corrosion casts*, British Journal of Cancer, 80 (1999), pp. 724–732.

[36] S. Modok, P. Hyde, H. Mellor, T. Roose, and R. Callaghan, *Diffusivity and distribution of vinblastine in three-dimensional tumour tissue: Experimental and mathematical modelling*, European Journal of Cancer, 42 (2006), pp. 2404–2413.

[37] A. Pries, K. Ley, M. Claassen, and P. Gaehtgens, *Red cell distribution at microvascular bifurcations*, Microvasc. Res., 38 (1989), pp. 81–101.

[38] A. Pries, D. Neuhaus, and P. Gaehtgens, *Blood viscosity in tube flow: dependence on diameter and hematocrit*, Am. J. Physiol., 263 (1992), pp. H1770–H1778.

[39] A. Pries and T. Secomb, *Microvascular blood viscosity in vivo and the endothelial surface layer*, Am. J. Physiol. Heart Circ. Physiol., 289 (2005), pp. H2657–H2664.

[40] P. Rand, E. Lacombe, H. Hunt, and W. Austin, *Viscosity of normal human blood under normothermic and hypothermic conditions*, Journal of Applied Physiology, 19 (1964), pp. 117–122.

[41] B. Rippe, A. Kamiya, and B. Folkow, *Simultaneous measurements of capillary diffusion and filtration exchange during shifts in filtration-absorption and at graded alterations in the capillary permeability surface area products (PS).*, Acta Physiol Scand, 104 (1978), pp. 318–36.

[42] E. Sevick and R. Jain, *Measurement of capillary filtration coefficient in a solid tumor*, Cancer Res, 51 (1991), pp. 1352–1355.

[43] E. Swabb, J. Wei, and P. Gullino, *Diffusion and Convection in Normal and Neoplastic Tissues*, Cancer Research, 34 (1974), p. 2814.

[44] R. Penta, D. Ambrosi, and A. Quarteroni, *Multiscale homogenization for fluid and drug transport in vascularized malignant tissues*, Mathematical Models and Methods in Applied Sciences, 25 (2015), p. 79–108.

List of Figures

6 Tables

Parameter	Value	Units	Formula	Description
Geometrical and Physiological Parameters				
s	100	μm	/	Arteriole and venule length scale
L	1	cm	/	Chamber length scale
d_2	50	μm	/	Capillary length scale (region 2)
μ	4×10^{-3}	kg/m/s	/	Viscosity of blood
k^{int}	0.4	μm^2	/	Permeability of the interstitium
$R_a = R_v$	10^{-2}	/	/	"Leakiness" of the arterioles and venules
k_2	37.4	μm^2	/	Permeability of the region 2 capillary network
h	37.4	μm^2	/	Permeability of the arteriole and venule networks
$S_a/V_a = S_v/V_v$	6.47×10^{-4}	μm^{-1}	/	Surface area to volume ratio
$S_a/V_p = S_v/V_p$	9.86×10^{-5}	μm^{-1}	/	Surface area to volume ratio
Length Scale Ratios				
ν	5×10^{-2}	/	d/s	Length scale ratio
η	0.1	/	s/L	Length scale ratio
Modelling Parameters				
n	0.152	/	V_a/V_p	Volume ratio
r	0.986	/	$\mu L_a L^4 S_a/V_p s^4$	Modelling ratio
C	4×10^{-9}	m^2	$k^{int}L^2/s^2$	Modelling ratio
P_{mal}	9.36×10^{-12}	m^2	$k_{\text{mal}}L^2 d_{\text{mal}}^2/s^4$	Modelling ratio

Table 1: A table of the fixed parameters

Network	Grid-I	Grid-II	Grid-III	Grid	Irregular-II	Irregular-I	Grid-IV	Hexagons
V_t/V_c	1.6933	2.4458	3.6812	4.2632	4.4358	6.0295	6.0571	6.5651

Table 2: The values of V_t/V_c for each explicit network under consideration

7 Figures

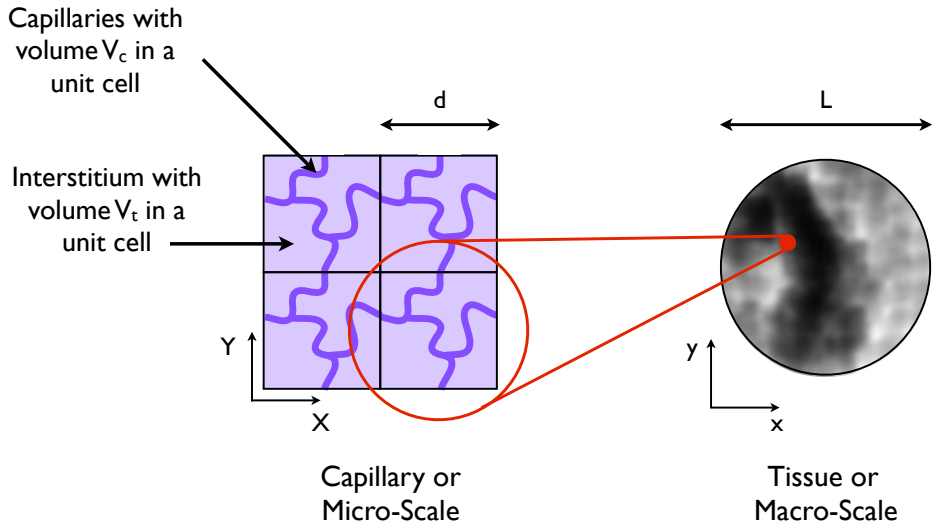

Figure 1: On the left-hand side is a 2D schematic of a cross-section through a tissue on the capillary or micro- length scale. The capillaries and interstitium are dark and light purple, respectively. A single periodic unit is highlighted in red. The total volume of this unit is denotes V, whilst the capillary and interstitial volumes are V_c and V_t, respectively. The right-had side depicts the macro-scale, where the distribution of fluid and mass appears as a 'grey-scale' and can be modelled as a continuum.

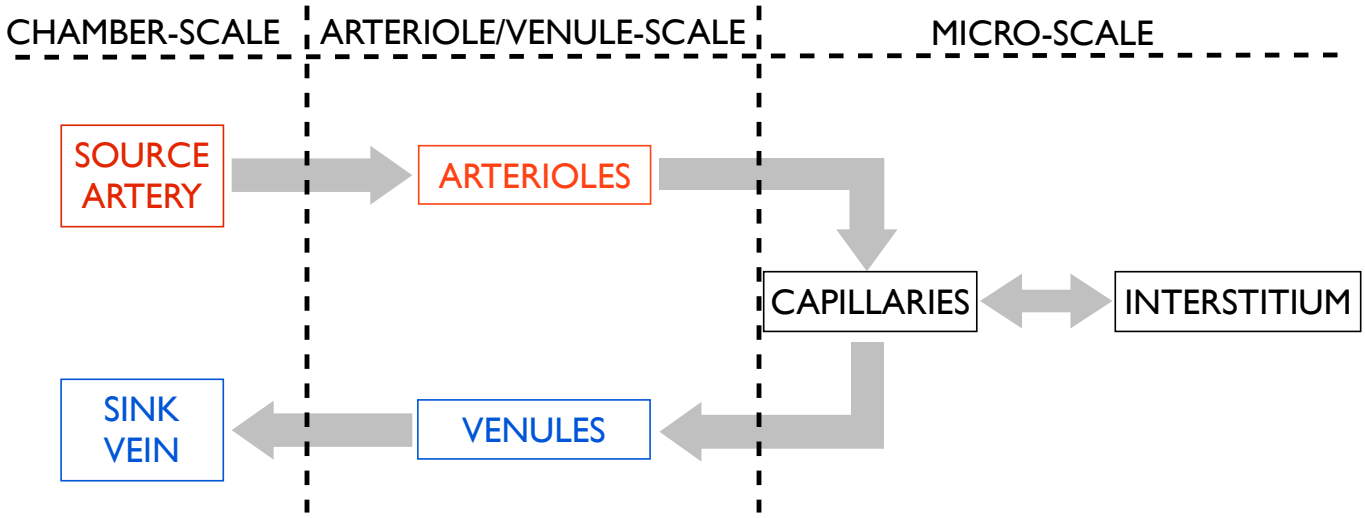

Figure 2: The fluid pathway. Fluid flows from a source artery, through the arterioles into the capillaries, and then out of the chamber through a sink vein via the venules. Since the capillaries are leaky there may also be fluid exchange between the capillaries and the interstitium.

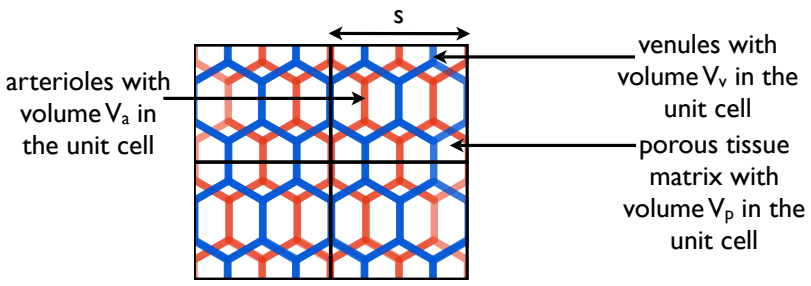

Figure 3: A schematic of a cross-section through the tumour on the length scale of the arterioles and venules. The arterioles, venules and porous tissue matrix (comprised of the capillary bed and interstitium) are in red, blue and white, respectively. The arteriole, venule and porous tissue volumes in a unit cell are denoted V_a, V_v and V_p, respectively.

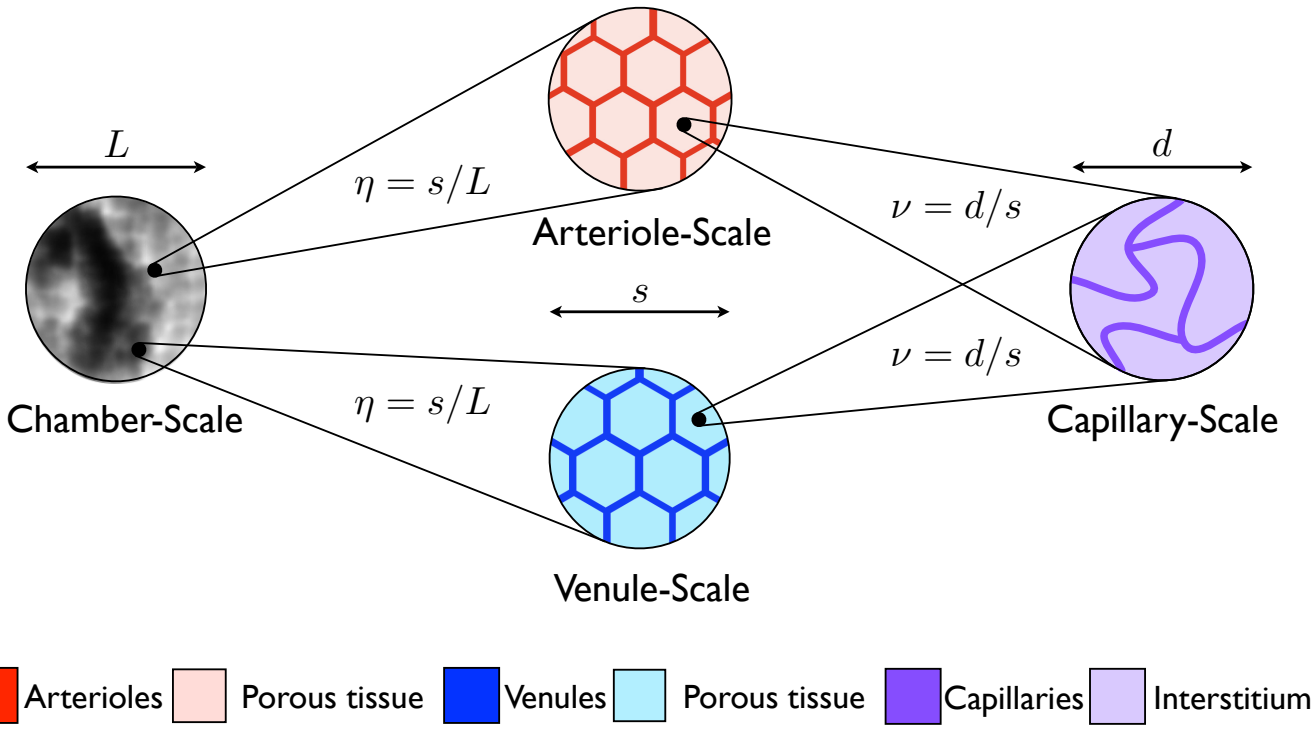

Figure 4: The three characterizing length scales are the micro-scale of the capillaries ($d \approx 50\mu$m), the arteriole/venule-scale ($s \approx 10^3\mu$m), and the chamber-scale ($L \approx 10^4\mu$m). These three length scales interact through the dimensionless ratios $\nu = d/s$ and $\eta = s/L$.

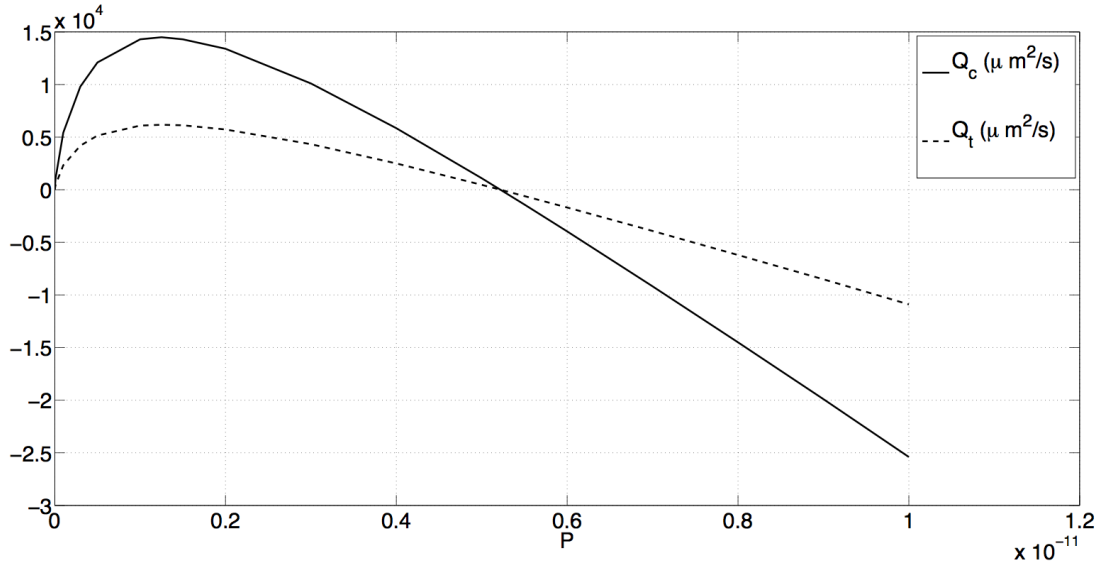

Figure 5: A plot of Q_c and Q_t (both measured in $\mu \mathrm{m}^2/s$) against the parameter P (measured in m^2) that captures the permeability and density of the capillary network.

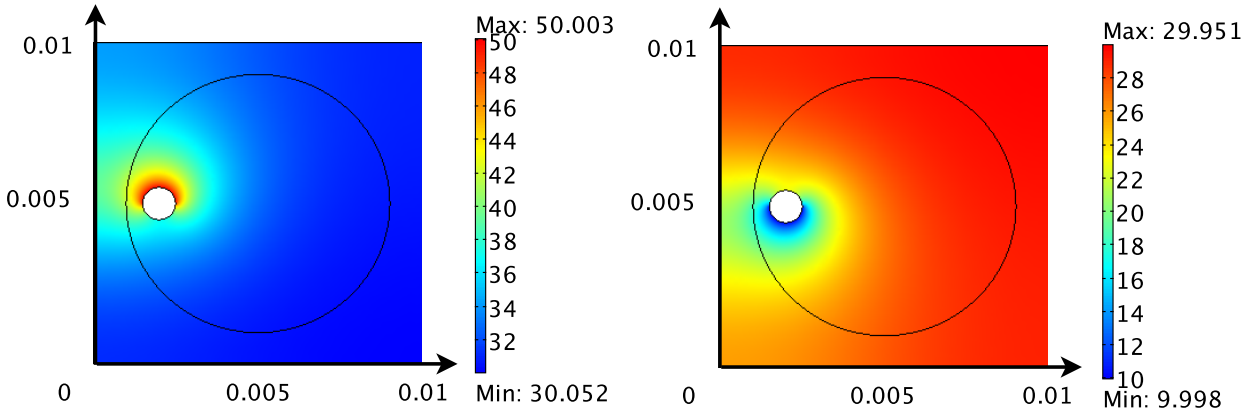

(a) p_a (b) p_v

Figure 6: The solutions for p_a and p_v when $P = 1 \times 10^{-14}\,\mathrm{m}^2$. Chamber dimensions are metres, and all pressures are given in units of mmHg.

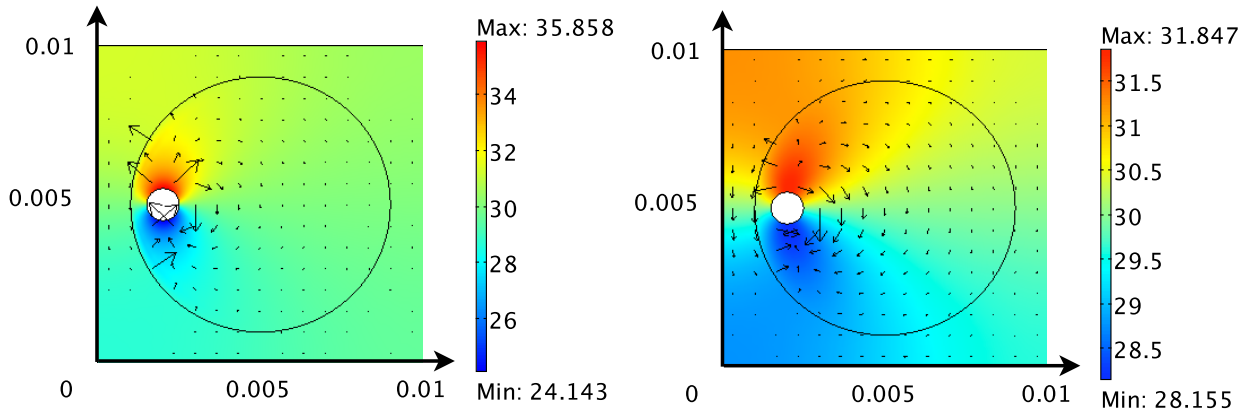

(a) $P = 1 \times 10^{-14}$

(b) $P = 1.25 \times 10^{-12}$

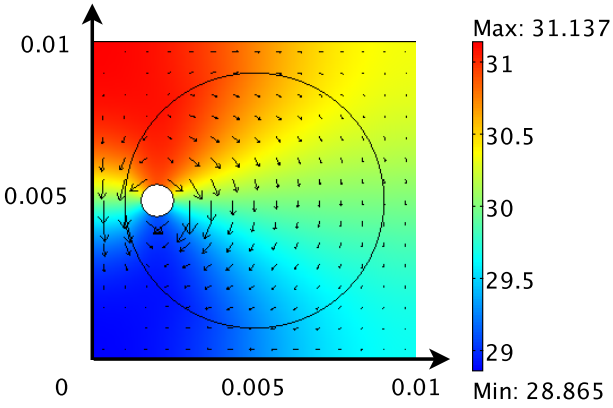

(c) $P = 5.2 \times 10^{-12}$

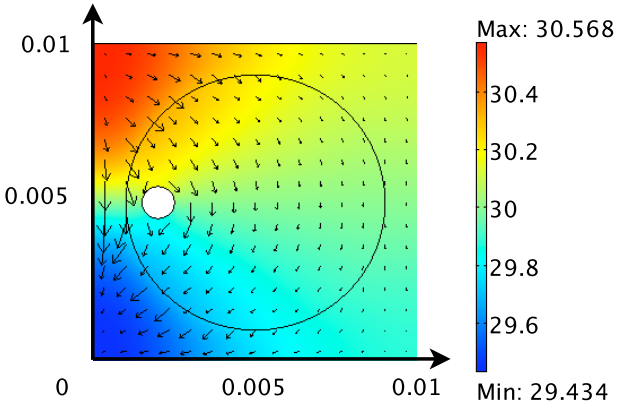

(d) $P = 1 \times 10^{-10}$

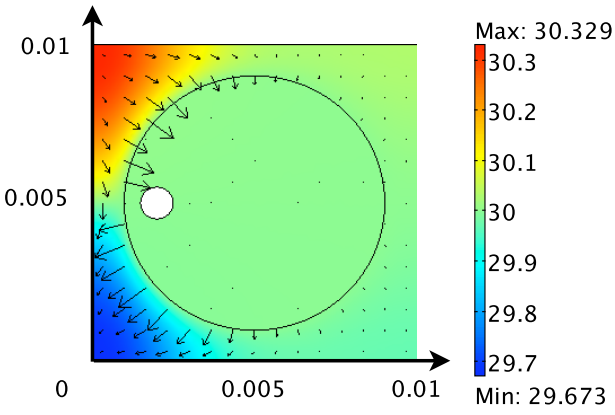

(e) $P = 1 \times 10^{-8}$

Figure 7: The solutions for $p_c = p_t$ for various values of P. Chamber dimensions are metres, and the arrows represent $\mathbf{u}_c$ (arrow length is proportional to the magnitude of the velocity vector). All pressures are given in units of mmHg.

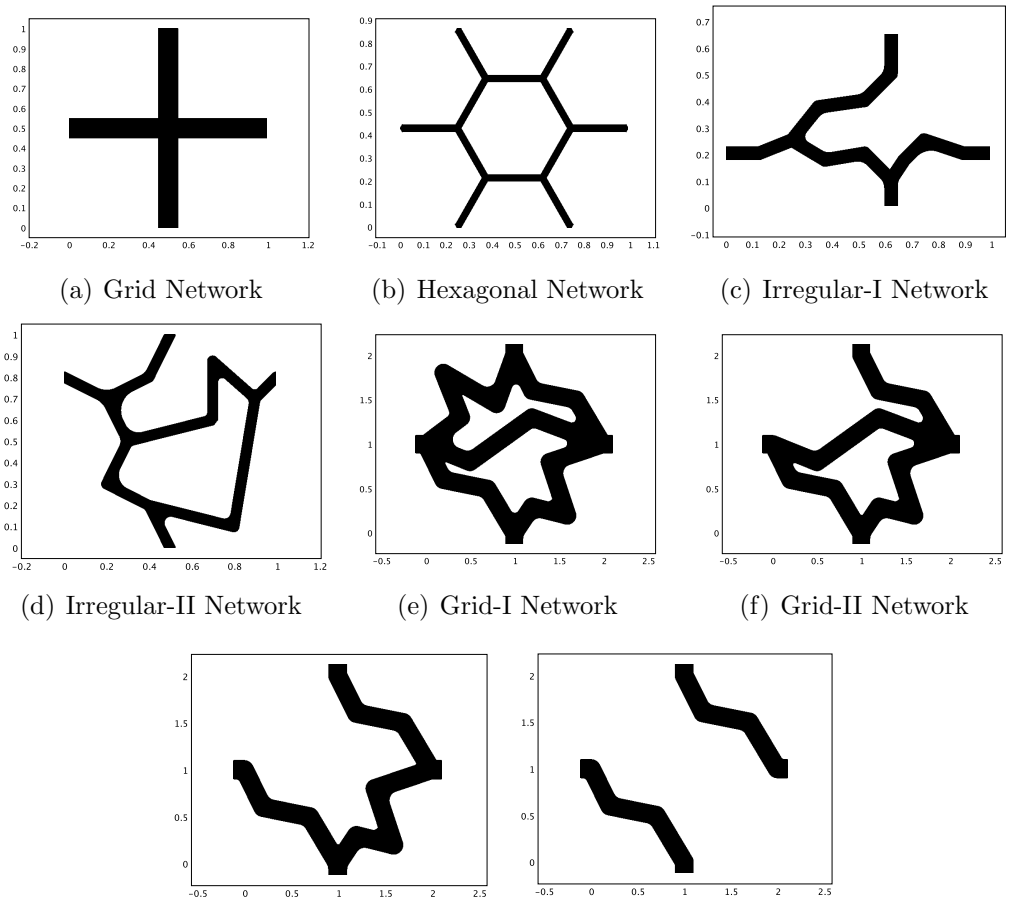

(a) Grid Network (b) Hexagonal Network (c) Irregular-I Network

(d) Irregular-II Network (e) Grid-I Network (f) Grid-II Network

(g) Grid-III Network (h) Grid-IV Network

Figure 8: Some explicit network examples.

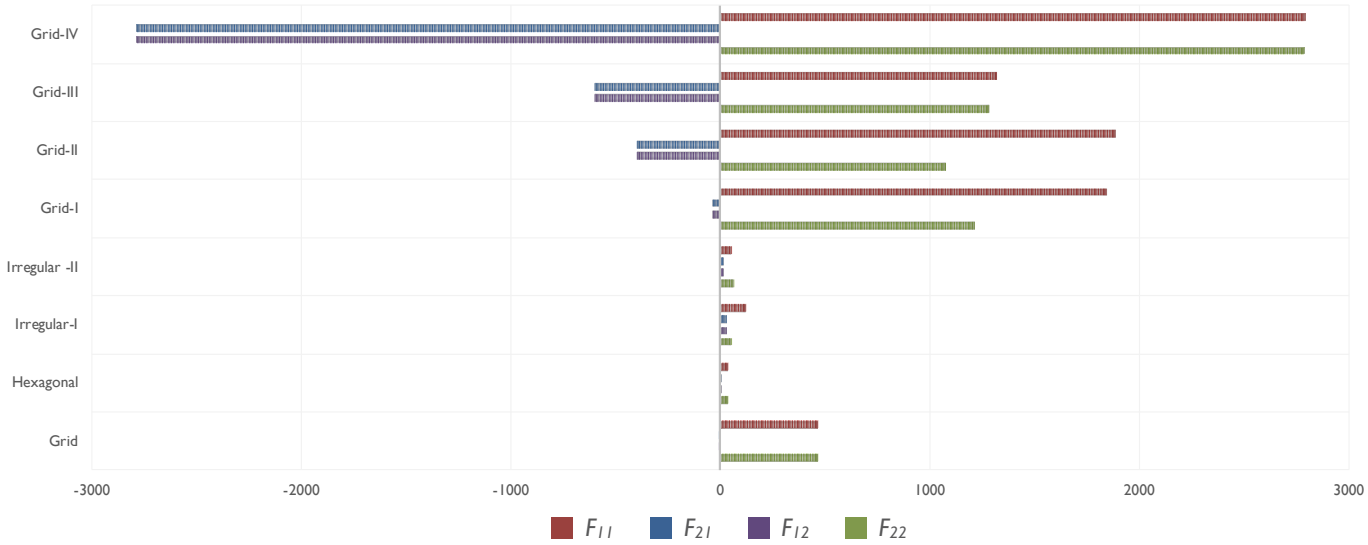

(a) F_{ij} (μm^2)

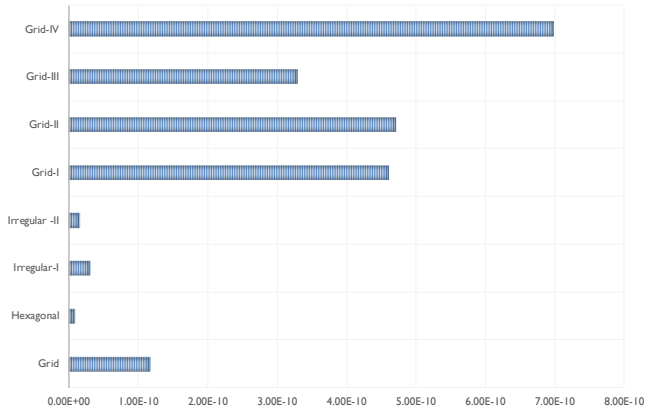

(b) P-values (m^2)

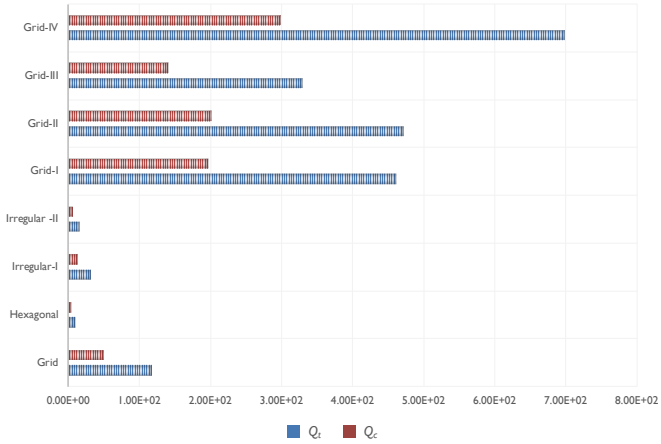

(c) Q_t and Q_c (both in μm^2/s)

Figure 9: The P-values and corresponding values of Q_c and Q_t for each of the explicit networks of Figure 8.

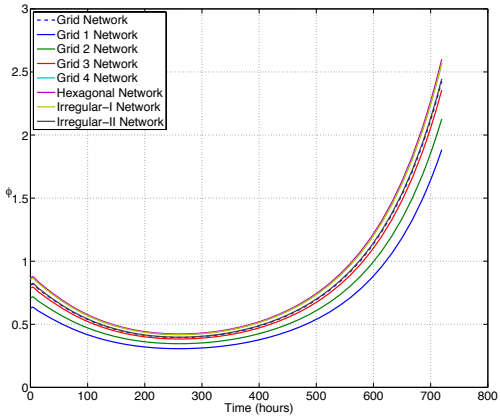

(a) $K = 1/29$ hours^{-1}: Single Injection

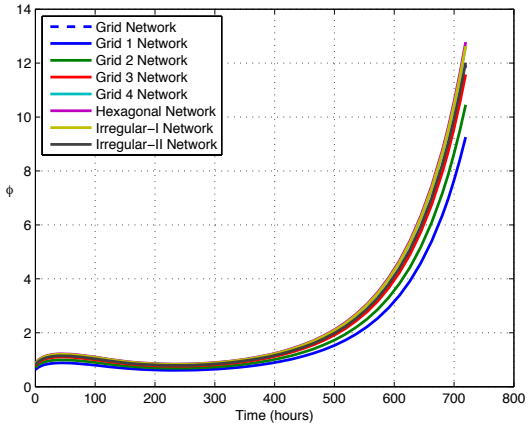

(b) $K = 1/29$ hours^{-1}: Constant Perfusion

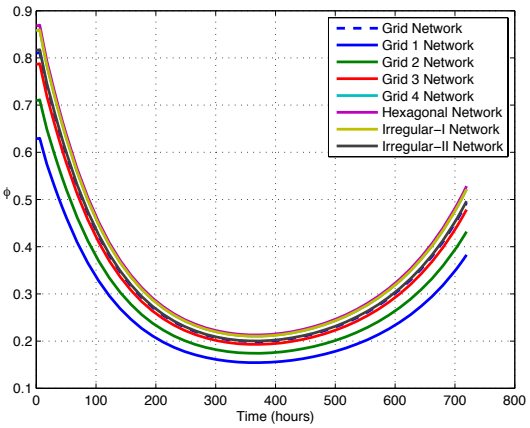

(c) $K = 1/31$ hours^{-1}: Single Injection

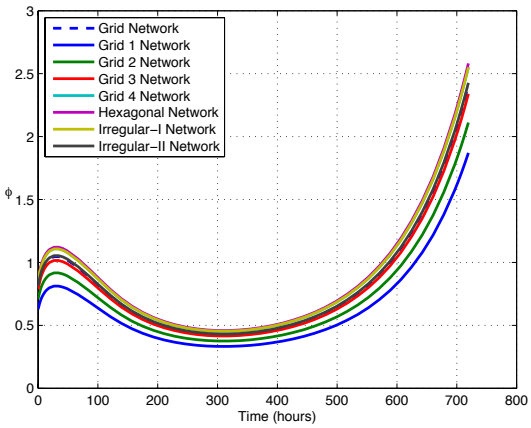

(d) $K = 1/31$ hours^{-1}: Constant Perfusion

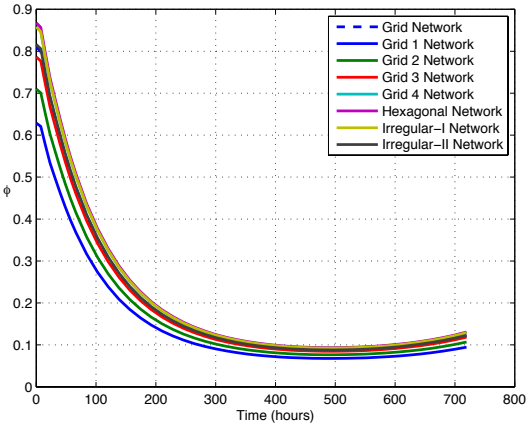

(e) $K = 1/33$ hours^{-1}: Single Injection

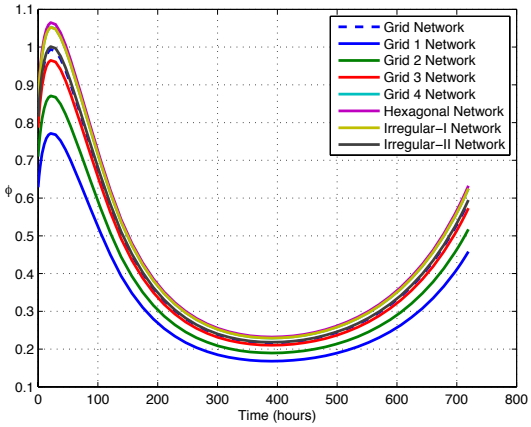

(f) $K = 1/33$ hours^{-1}: Constant Perfusion

Figure 10: The variation of the average interstitial volume fraction as a function of time.

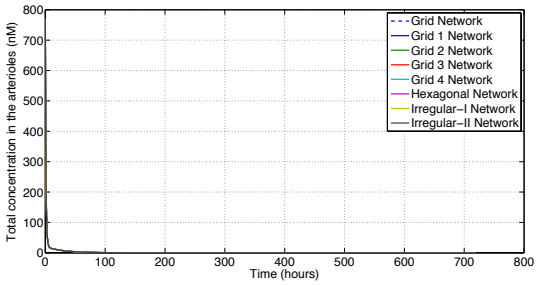

(a) Average vinblastine concentration in the arterioles as a function of time

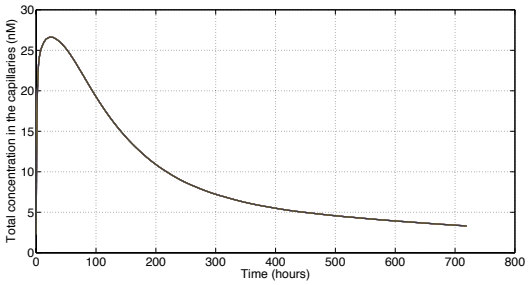

(b) Average vinblastine concentration in the capillaries as a function of time

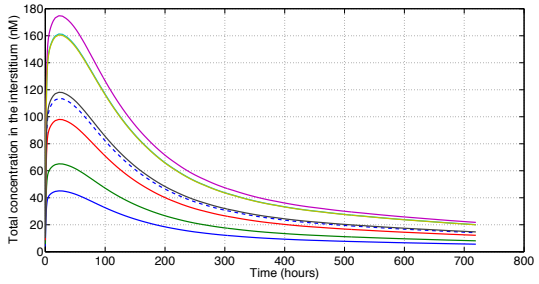

(c) Average vinblastine concentration in the interstitium as a function of time

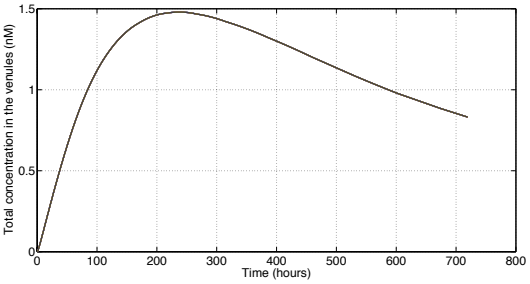

(d) Average vinblastine concentration in the venules as a function of time

Figure 11: The average vinblastine concentration in each of the arterioles, capillaries, interstitium and venules for a single injection.

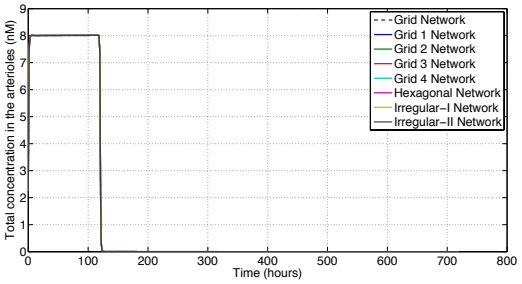

(a) Average vinblastine concentration in the arterioles as a function of time

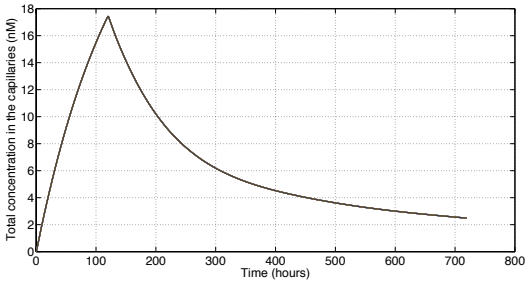

(b) Average vinblastine concentration in the capillaries as a function of time

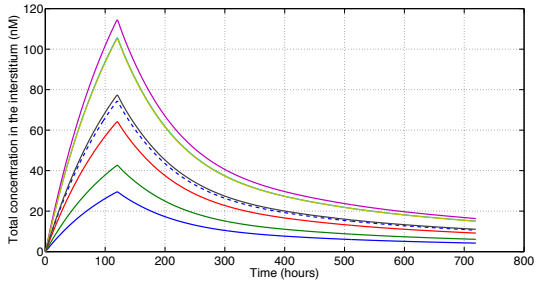

(c) Average vinblastine concentration in the interstitium as a function of time

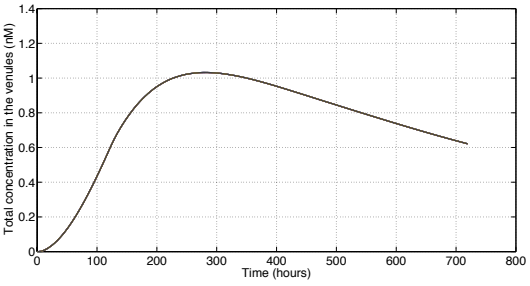

(d) Average vinblastine concentration in the venules as a function of time

Figure 12: The average concentration in each of the arterioles, capillaries, interstitium and venules for constant perfusion.